MULTISCALE MODEL. SIMUL.
Vol. 8, No. 4, pp. 1178–1211

TRACING DIFFUSION IN POROUS MEDIA WITH FRACTAL PROPERTIES*

IGOR G. VLADIMIROV† AND A. Y. KLIMENKO‡

Abstract. This work is concerned with conditional averaging methods which can be used for modeling of transport in porous media with volume reactions in the fluid phase and surface reactions at the fluid/solid interface. The model under consideration takes into account convection, diffusion within the pores and on larger scales, and homogeneous and heterogeneous reactions. Near the interface with fractal properties, the fluid flow is slow, and diffusion, as a transport mechanism, dominates over convection. Following the conditional moment closure paradigm, we employ a diffusion tracer as a reference scalar field that makes the conditional averaging sensitive to the proximity of a point to the interface. The resulting conditionally averaged reactive transport equations are governed by the probability density function (PDF) of the diffusion tracer, and this makes the study of its behavior an important problem. We consider a hitting time stochastic interpretation of the diffusion tracer, establish integral equations relating it to a subsidiary distance tracer, and obtain distance-diffusion inequalities. Assuming that the fluid/solid interface and pores themselves possess fractal properties which are quantified, in particular, by a variant of the Minkowski–Bouligand fractal dimension, we investigate the interplay between the interface and network scenarios of fractality in the scaling laws of the diffusion tracer PDF. We also discuss and employ several hypotheses, including a lognormal cascade hypothesis on the behavior of the diffusion tracer at different length scales.

Key words. reactive transport, porous media, self-similarity, contact distribution, fractal dimension, conditional averaging, diffusion tracer, scaling laws, lognormal cascade hypothesis

AMS subject classifications. Primary, 76S05, 76V05, 76M35, 76M55, 80A32; Secondary, 60G18, 60G40, 60G60, 60J60, 60J65, 35J05, 31B10

DOI. 10.1137/090760234

1. Introduction.

A distinguishing feature of reactive transport phenomena in porous media is high irregularity of spatial structures through which the fluid phase flows. Although the geometric details are unique on short length scales for any particular sample, their effects interact and add up together to produce a macroscopically stable signature of the material.

A typical setting is a two-component medium whose "skeleton" is formed by a solid phase, often referred to as the solid matrix, with the rest of the physical space occupied by reacting liquids or gases. The latter can also react with the "walls" of the solid, and, since their area per unit volume of the porous medium is usually large, the surface reactions can be dominant to the extent that the pores play an ancillary, though indispensable, role of networked channels for delivery of reactants. It is due to the largeness of the internal surface that porous media are extensively employed in chemical engineering applications.

A principal technique of modeling reactive transport in porous media is volume averaging [32] whereby velocities and concentrations are replaced by their local spatial averages and the momentum and mass transport equations are appropriately modified

*Received by the editors May 27, 2009; accepted for publication (in revised form) April 2, 2010; published electronically June 29, 2010. This work was supported by the Australian Research Council.
http://www.siam.org/journals/mms/8-4/76023.html

†School of Engineering, The University of Queensland, Brisbane, QLD 4072, Australia. Current address: School of Engineering and Information Technology, University of New South Wales at the Australian Defence Force Academy, Canberra, ACT 2600, Australia (i.vladimirov@adfa.edu.au).

‡Corresponding author. School of Engineering, The University of Queensland, Brisbane, QLD 4072, Australia (a.klimenko@uq.edu.au).

to make them more amenable to theoretical analysis. The simplified form acquires dependence on the bulk parameters of the porous medium such as porosity and specific internal surface area [13].

The conventional volume averaging, however, evens out different points of the fluid phase, thus neglecting the unequal accessibility of the internal surface and distorting the relative contribution of surface/volume reactions. The distortion can be particularly noticeable in materials with fractal properties [3, 8, 20, 21], where both the fluid/solid interface and the pores themselves exhibit self-similar "ruggedness" in a wide range of length scales which amount to a significant portion of the fluid phase volume. The subtle interplay between the coexisting *interface* and *network* scenarios of fractality generates hierarchies of layers in the fluid phase so that local properties of transport are uniform within the same layer and vary in a cascade manner from one layer to another.

A refined approach to volume averaging consists in replacing the underlying fields by their ensemble averages conditioned on a tracer scalar which, being strictly positive in the fluid phase and gradually vanishing towards the interface, quantifies the proximity of a point in the fluid phase to the solid matrix. Relying on the machinery of random fields [11], the ensemble averages, in general, retain dependence on the location and, therefore, room for spatially nonhomogeneous settings. There are many different ways to introduce such a tracer, and apparently the most straightforward of them is provided by the usual Euclidean distance. Despite its advantageous simplicity, however, the *distance tracer* overlooks deeply hidden parts of the fluid/solid surface. Such cavities may, nevertheless, be well reachable by a diffusion process which, due to its erratic sample paths, constitutes the main transport mechanism in small pores. Therefore, although the distance tracer is convenient for quantifying the fractal properties of porous media, the interface-sensitive conditioning should employ a tracer scalar defined as a solution to a Poisson equation with negative constant right-hand side in the fluid phase and zero boundary condition, that is, the simplest elliptic partial differential equation (PDE) interpreted as a reaction-diffusion equation. Using the *diffusion tracer* as a reference field for conditional averaging is the main ingredient of the conditional moment closure (CMC) method [18] and its adaptation to modeling of transport in porous media, PCMC [17]. Another similar conditioning scalar—the marker scalar—was previously introduced by Bilger [6] for conditional transport equations in application to premixed combustion. The resulting conditionally averaged reactive transport equations are essentially governed by the probability density function (PDF) of the diffusion tracer, and this makes the study of its behavior an important problem. While conditioning on the diffusion tracer seems to be most suitable for characterization of transport of diffusing scalars, we think that conditioning on the distance tracer can be efficient for characterization of the pressure-induced transport in fractal porous media. Thus, relating characteristics of diffusion and distance tracers to each other and to the fractal properties of the media is the key question for accurate modeling of reacting/adsorbing flows in multiscale porous media.

The present paper is aimed at investigating the influence of the fractal properties of the porous medium on the behavior of the diffusion tracer PDF and on joint characteristics of the diffusion tracer and the distant tracer. To this end, we consider a stochastic representation of the diffusion tracer by the expected value of the time needed for a three-dimensional standard Wiener process [25], starting from a given point in the fluid phase, to hit the solid matrix. The *first hitting time* interpretation renders the diffusion tracer as a temporal measure of proximity to the solid matrix in

terms of the simplest Markov diffusion in the physical space. Due to martingale properties of the Wiener process, the diffusion tracer also quantifies the spatial proximity to the fluid/solid interface. To this end, we establish integral equations that relate it with the distance tracer and obtain distance-diffusion inequalities.

Assuming that the fluid/solid interface and the pores themselves possess fractal properties which are quantified by a *contact dimension* of the interface, a variant of the Minkowski–Bouligand fractal dimension [7] related to the distance tracer, and by a *network fractality parameter*, we investigate the interplay between the interface and network scenarios of fractality. This allows a power law to be established for the PDF of the diffusion tracer that constitutes the main result of the present study. The treatment of the network fractality is accomplished using the partition of the fluid phase into basins of attraction to local maxima of the diffusion tracer along a subsidiary gradient flow associated with the tracer. The size of the resulting "chunks" of the fluid phase is a piecewise constant field which allows the diffusion and distance tracers to be scaled in order to "decouple" the relative proximity to the interface from the pore largeness.

Due to the complexity of the underlying problem, the analysis unavoidably, at least at the current stage, employs, apart from rigorous results and constructs, additional hypotheses which should be considered as heuristics for further development. These include a *network distance-diffusion scaling* hypothesis pertaining to the network fractality of the porous medium; an *isolation of relative scales* hypothesis which stochastically decouples the effects of interface and network scenarios; and, finally, a *lognormal cascade* hypothesis on the conditional distribution of the relative diffusion tracer with respect to the relative distance tracer at different length scales, analogous to the lognormal energy cascade conjectured in the statistical theory of turbulence [19].

The paper is organized as follows. Section 2 describes the reactive transport equations in a two-component porous medium and introduces the diffusion tracer. Section 3 outlines ensemble averaging whose comparison with volume averaging and related homogeneity and ergodicity considerations are provided by Appendix A. Section 4 formulates the conditionally averaged transport equations of the PCMC approach of [17] based on an ensemble version of the spatial averaging theorem [32, p. 10], which we establish in Appendix B using subsidiary interface and inflow operators. Section 5 qualitatively discusses fractal properties of porous media. These are quantified in section 6 by the interface contact dimension in terms of the distance tracer. Section 7 studies the hitting time interpretation of the diffusion tracer and establishes an inequality between the distance and diffusion tracers whose strengthened version is provided by Appendix D. Higher moments of the first hitting time, forming a recurrence sequence of diffusion tracers, are considered in Appendix C. Section 8 derives integral equations relating the distance and diffusion tracers. Section 9 introduces the partition of the fluid phase into basins of attraction to the local maxima of the diffusion tracer and formulates the network distance-diffusion scaling hypothesis. A related maximum localization principle is established in Appendix E. Section 10 considers the interplay between the network and interface scenarios of fractality under the isolation of relative scales hypothesis which is directly verified in Appendix F for the case of spherical pores along with the network distance-diffusion scaling hypothesis. Section 11 formulates the lognormal hypothesis on the conditional distribution of the relative diffusion tracer with respect to the relative distance tracer that allows the unconditional PDF to be studied in Appendix G using Laplace's method [9]. The combined contribution of the interface and network scenarios of fractality to the power

law for the diffusion tracer PDF and its implication for the conditional dissipation rate are considered in section 12. Section 13 provides concluding remarks.

2. Reactive transport equations. We consider a two-component porous medium formed by the solid matrix and the fluid phase. The latter occupies a fixed open subset Φ of the physical space and may consist of several, say s, reacting species. In the framework of the Lagrangian picture of fluid dynamics, the reactants are transported in two ways: (1) convectively with the flow, that is, "aboard" fluid parcels, and (2) via diffusion, which can be viewed as the fluid parcels exchanging their "passengers." Whereas "commuting" from one fluid parcel to another is a relatively slow way of traveling in comparison with convection in the fast flow far from the solid matrix, diffusion is the main transport mechanism in the vicinity of the interface $\partial\Phi$ where the flow creeps over small-scale obstacles.

The transport is accompanied by changes in the amounts of constituent species due to chemical reactions which develop both in the volume and at the internal surface. Not restricting our attention to the setting where the fluid phase does not penetrate the solid matrix, we also include in our treatment reactions in a thin film of a few molecular layers at the surface, for example, adsorption. Thus, at the extremes, there is a large-scale fast flow with convection as a main transport mechanism and exclusively volume reactions in the deep interior of Φ, and a small-scale flow almost at rest with predominantly diffusion transport which directly caters to surface reactions at the boundary $\partial\Phi$.

The state of the fluid phase is described by several scalar and vector fields. These include the total density of the fluid phase ρ, the mass fractions of the fluid reactants $Y_1, \dots, Y_s$, and the fluid velocity v. By their physical meaning, the fields are functions of time t and of the spatial vector variable x running over the set Φ. However, in order to deal with *superficial averages* over the whole space, we formally extend the fields by padding them with zero values on the complement $\Phi^{\mathrm{C}} := \mathbb{R}^3 \setminus \Phi$ occupied by the solid matrix. The conservation of mass of the fluid phase as a whole is described in the divergence form by

$$\partial_t \rho + \operatorname{div}(\rho v) = 0, \tag{2.1}$$

where ρv is the overall mass flux which vanishes at the interface $\partial\Phi$ only if the fluid phase does not penetrate the solid and the nonslip boundary condition of the viscous flow holds. The reactive transport equations for the constituent species are

$$\partial_t(\rho Y_k) + \operatorname{div}(\rho v Y_k) - \underbrace{\operatorname{div}(\rho D_k \nabla Y_k)}_{\text{diffusion}} = \underbrace{\rho W_k}_{\text{reaction}}, \qquad k = 1, \dots, s, \tag{2.2}$$

or, in an equivalent alternative form,

$$\rho \partial_t Y_k + \underbrace{\rho v \cdot \nabla Y_k}_{\text{convection}} - \operatorname{div}(\rho D_k \nabla Y_k) = \rho W_k. \tag{2.3}$$

Here, $\rho v \cdot \nabla Y_k$, with $u \cdot w$ standing for the scalar product, is what is left of $\operatorname{div}(\rho v Y_k)$, the divergence of the convective mass flux of the kth species, as a result of the reduction $\partial_t(\rho Y_k) + \operatorname{div}(\rho v Y_k) = \rho \partial_t Y_k + \rho v \cdot \nabla Y_k$ following from (2.1). The problem of multicomponent diffusion is not considered here and, according to Fick's law, $-\rho D_k \nabla Y_k$ is the mass flux of the kth species due to diffusion, with D_k the diffusivity of this species; and W_k is the formation rate of the kth species in volume reactions, which

depends nonlinearly on $Y_1, \dots, Y_s$, that is, $W_k = W_k(\mathbf{Y})$, where the specific form of these functions depends on particularities of the chemical kinetics. Apart from the bulk equation (2.3), the fractions $Y_1, \dots, Y_s$ obey boundary mass balance equations for surface reactions at the interface $\partial\Phi$. The appropriate surface reaction rates are denoted by $S_1, \dots, S_s$, with S_k understood as the mass of the kth reactive species produced locally per unit area of the interface and per unit time. Their part will be discussed in more detail in section 4.

In addition to the mass fractions of reactants, we follow [17, section 3] by also introducing an ancillary scalar field $Z := Y_0$ which vanishes in the solid matrix, $Z|_{\Phi^{\mathrm{C}}} = 0$, and which, in the fluid phase set Φ, is governed by a PDE similar to (2.3):

$$\rho\partial_t Z + \rho v \cdot \nabla Z - \operatorname{div}(\rho D_0 \nabla Z) = \rho W_0. \tag{2.4}$$

Unlike $Y_1, \dots, Y_s$ associated with actual reactants, Z is interpreted as the mass fraction of a virtual species with diffusivity D_0 and positive formation rate W_0 in the fluid phase. The species plays the role of a dye produced in the fluid phase and absorbed by the solid matrix, so that its local fraction Z, abundant in the deep interior of Φ, gradually approaches zero towards the interface $\partial\Phi$ (that is, $Z = 0$ at $\partial\Phi$), thus tracing the dye and quantifying the proximity to the solid matrix. Therefore, Z can be used as a reference scalar field for conditional ensemble averaging in order to make the latter sensitive to the qualitatively different convection-driven and diffusion-driven regimes of reactive transport above.

3. Ensemble averaging. Due to the highly irregular spatial structure of a typical porous medium, the set Φ, occupied by the fluid phase, can be regarded as a random set [15, 24]. Accordingly, its indicator function

$$\beta(x) := \mathcal{I}_\Phi(x) := \begin{cases} 1 & \text{for } x \in \Phi, \\ 0 & \text{otherwise} \end{cases} \tag{3.1}$$

is best modeled as a realization of a random field [11, 22]. If β is (spatially) homogeneous (or, interchangeably, stationary) in the sense that its multipoint probability distributions are invariant under translations of the physical space, then the ensemble average

$$\varphi(x) := \langle \beta(x) \rangle = \mathsf{P}(x \in \Phi), \tag{3.2}$$

with P the underlying probability measure, is constant in x and quantifies the ensemble fraction of the fluid phase. The latter coincides with the volume fraction, known as *porosity*, under the *ergodicity* assumption discussed in Appendix A. Unconditional averaging methods constitute an established set of tools for multiphase systems [12], including, for example, hydrogeological models [23].

4. Conditionally averaged transport equations. Regarding the reactant mass fractions $Y_1, \dots, Y_s$ and the other scalar- and vector-valued functions of time t and of spatial vector variable x, introduced in sections 2 and 3, as random fields and following [17], we will use their density-weighted conditional Favre averages with respect to Z denoted by overbars,

$$\overline{Y_k} := \langle \rho Y_k \mid Z = z \rangle \,/\, \langle \rho \mid Z = z \rangle \,. \tag{4.1}$$

These reduce to $\langle Y_k \mid Z = z \rangle$ if ρ is a nonrandom function of Z, which is the case, for example, for incompressible fluids where $\rho = \text{const}$. Here, the numerator and

denominator are understood in the sense of ensemble averaging, discussed in section 3, at a fixed but otherwise arbitrary point (t, x) of the time-space, conditioned on a given positive level z for the diffusion tracer $Z(t, x)$, so that $\overline{Y_1}, \ldots, \overline{Y_s}$, defined by (4.1), are functions of t, x, and z. Recalling that Z vanishes everywhere in the solid matrix and is positive in the fluid phase Φ, the assumption $z > 0$ singles out those realizations of Φ which satisfy $x \in \Phi$. The association with the fluid phase is, however, where the analogy with the intrinsic volume averages ends. Indeed, being conditioned on Z, the conditional ensemble averages take into account the proximity of x to the solid matrix.

For what follows, we denote by P_Z the conditional PDF of the diffusion tracer Z at a given time-space point (t, x), provided that $x \in \Phi$. Due to the latter condition, P_Z will be referred to as the *intrinsic* PDF of Z. From its definition, P_Z is a nonnegative function of t, x, and $z > 0$, satisfying the normalization condition $\int_0^{+\infty} P_Z \mathrm{d}z = 1$. The same properties hold for the density-weighted variant of the PDF defined by

$$\widetilde{P}_Z := P_Z \, \langle \rho \mid Z = z \rangle / \langle \rho \mid Z > 0 \rangle,$$

where $\langle \rho \mid Z > 0 \rangle = \langle \beta\rho \rangle / \varphi$, and use is made of (3.1) and (3.2) whereby $\mathsf{P}(Z(t, x) > 0) = \varphi(x)$ and $\langle \beta\rho \rangle$ is the superficial ensemble average of the fluid density ρ. The PDFs $\widetilde{P}_Z$ and P_Z coincide, for example, in the incompressible case. In view of the frequent appearance of $\langle \beta\rho \rangle$ as a multiplier of $\widetilde{P}_Z$ in the following equations, we will use the shorthand notation

$$P := \langle \beta\rho \rangle \widetilde{P}_Z = \varphi \langle \rho \mid Z = z \rangle P_Z.$$

Note that the function P satisfies a different normalization $\int_0^{+\infty} P \mathrm{d}z = \langle \beta\rho \rangle$. Moreover, for any nonrandom function f which is nonzero only on the positive half-axis $(0, +\infty)$, the relation

$$\int_0^{+\infty} \overline{S} f(z) P \mathrm{d}z = \langle \rho S f(Z) \rangle \tag{4.2}$$

holds for any random field S whose conditional Favre average $\overline{S}$ is defined similarly to (4.1). In fact, the fulfillment of (4.2) for any such test function f is an equivalent, though implicit, definition of $\overline{S}$. Furthermore, applied to infinitely differentiable test functions f whose support is bounded and contained by the positive half-axis, the observation allows the following equation to be deduced from (2.1) and (2.4):

$$\partial_t P + \operatorname{div} \big(\overline{v} P + \partial_z (\overline{D_0 \nabla Z} \, P) \big) + \partial_z (\overline{W_0} \, P) + \partial_z^2 (\overline{N} P) = 0, \tag{4.3}$$

where div and ∇ act in the spatial variables x only, and $\overline{N}$ is the conditional Favre average of the dissipation rate

$$N := D_0 |\nabla Z|^2. \tag{4.4}$$

By similar reasoning, (2.1), (2.2), and (2.4) imply

$$\begin{aligned} &\partial_t (\overline{Y_k} P) + \operatorname{div} \big((\overline{v Y_k} - \overline{D_k \nabla Y_k}) P + \partial_z (\overline{D_0 Y_k \nabla Z} P) \big) \\ &\qquad + \partial_z (\overline{W_0 Y_k} P) - \partial_z (\overline{(D_0 + D_k) \nabla Y_k \cdot \nabla Z} P) + \partial_z^2 (\overline{Y_k N} P) = \overline{W_k} P, \end{aligned} \tag{4.5}$$

where $\overline{W_1}, \ldots, \overline{W_s}$ are conditional Favre averages of the volume reaction rates. The terms $\partial_t(\cdot)$ and $\operatorname{div}(\cdot)$ of (4.3) and (4.5) vanish, for example, in the case of steady-state

spatially homogeneous random fields. The derivation of the conditionally averaged transport equations can be found in [18]. Following [17, section 4], the equations are coupled with boundary conditions which can be treated using the spatial averaging theorem [32, p. 10]. We provide its ensemble version in Appendix B for completeness of exposition. Employing the inflow operator Υ described in Appendix B, application of the theorem to (2.1) and (2.2) gives

$$\partial_t\langle\beta\rho\rangle + \operatorname{div}\langle\beta\rho v\rangle = \Upsilon(\rho v), \tag{4.6}$$

$$\partial_t\langle\beta\rho Y_k\rangle + \operatorname{div}\langle\beta\rho v Y_k\rangle = \langle\beta\rho W_k\rangle + \Upsilon(\rho v Y_k - \rho D_k\nabla Y_k) + \operatorname{div}\langle\beta\rho D_k\nabla Y_k\rangle, \tag{4.7}$$

where the last divergence originates from the diffusion term of (2.2). Integrating both parts of (4.3) over the positive values of z and using (4.2) and (4.6) yields

$$\big(\operatorname{div}(\overline{D_0\nabla Z}P) + \overline{W_0}P + \partial_z(\overline{N}P)\big)\big|_{z=0+} = \Upsilon(\rho v), \tag{4.8}$$

where the left-hand side corresponds to approaching the interface $\partial\Phi$ from the fluid phase. Similar reasoning applied to (4.5) and (4.7) gives the remaining boundary conditions

$$\Big(\operatorname{div}(\overline{D_0 Y_k\nabla Z}P) + \overline{(W_0 Y_k - (D_0+D_k)\nabla Y_k\cdot\nabla Z)}P + \partial_z(\overline{Y_k N}P)\Big)\Big|_{z=0+}$$

$$= \Upsilon(\rho v Y_k - \rho D_k\nabla Y_k). \tag{4.9}$$

The term on right-hand side of this equation represents the flux of scalar Y_k into the fluid phase; this flux can be related to heterogeneous chemical reaction or to sorption at the phase interface. As in the case of homogeneous reactions, specification of these rates is needed to obtain a closed formulation of the model. Under the approximation $\overline{Y_k N} \approx \overline{Y_k}\,\overline{N}$ (which neglects the conditional covariance of Y_k and N), and other analogous assumptions used in the CMC and PCMC approaches (details and justifications for these assumptions can be found in [18, 17]), (4.3) and (4.5) take the form

$$\partial_t P + \operatorname{div}(\overline{v}P) + \partial_z(\overline{W_0}P) + \partial_z^2(\overline{N}P) = 0, \tag{4.10}$$

$$\partial_t(\overline{Y_k}P) + \operatorname{div}(\overline{v}\,\overline{Y_k}P) + \partial_z\left(\overline{W_0 Y_k}P - \overline{N}P\partial_z\overline{Y_k} + \overline{Y_k}\partial_z(\overline{N}P)\right) = \overline{W_k}P, \tag{4.11}$$

while the interface conditions of (4.8) and (4.9) become

$$\big(\overline{W_0}P + \partial_z(\overline{N}P)\big)\big|_{z=0+} = \Upsilon(\rho v), \tag{4.12}$$

$$\big(\overline{W_0 Y_k}P - \overline{N}P\partial_z\overline{Y_k} + \overline{Y_k}\partial_z(\overline{N}P)\big)\big|_{z=0+} = \Upsilon(\rho v Y_k - \rho D\nabla Y_k). \tag{4.13}$$

Here we put $D_k = D_0 = D$—the problem of differential diffusion is not considered in the present work. Equation (4.11) can be solved for $\overline{Y_k}$, provided that its coefficients, P and $\overline{N}$, are known. The latter are constrained by (4.10) and depend on geometric properties of the porous media. In the present work, we are concerned with determining P and $\overline{N}$ for porous media with fractal properties. The properties of the model with respect to interface reactions is highly dependent on behavior of $\overline{N}$ close to the interface. This problem is complicated, and the rest of the paper is dedicated to determining properties of P and $\overline{N}$ for fractal porous media—without knowing these properties the PCMC model cannot be used in practice.

The fractality of the porous medium induces small-scale spatial fluctuations in the function Z near the interface. These fluctuations determine asymptotic behavior

of $\overline{N}$ near the interface (as $Z \to 0$). Together with the flow velocity v being small in the near-interface region (due to viscosity), this makes the Péclet number associated with the transport of the scalar field Z by (2.4) small: $\mathsf{Pe} \ll 1$. Thus, the convective term $\rho v \cdot \nabla Z$ of this PDE can be neglected in comparison with the diffusion term $\operatorname{div}(\rho D_0 \nabla Z)$. Hence, considering ρ, D_0, and W_0 to be constant and passing to the steady-state limit reduces (2.4) to the Poisson equation with zero boundary condition

$$\Delta Z = -W_0/D_0, \quad x \in \Phi, \text{ near } \partial\Phi; \qquad Z|_{\partial\Phi} = 0, \tag{4.14}$$

where Δ is the Laplace operator. In addition to being a steady-state reaction-diffusion equation, (4.14) allows Z to be interpreted in several other ways that complement the initial definition. One of them is that Z describes a stationary temperature field in the fluid phase as an isotropic medium (with a constant heat source over Φ) in thermal equilibrium with the solid matrix playing the role of a heat sink. In this thermal interpretation, the vector field $-\nabla Z$ is the heat flux, tangential to the *heatlines* [4]. Another interpretation links Z to the time needed for a Brownian motion to reach the solid matrix. This stochastic interpretation is considered in section 7 and allows scaling laws for Z to be related with fractal properties of the porous medium, which are discussed qualitatively in the next section and endowed with quantitative characteristics in section 6.

When diffusion is not the prime factor in the flow, another version of moment equations that involves conditioning on the distance tracer R is called PDCMC (porous distance-conditioned moment closure) and can be easily derived using standard conditional techniques [18, 17]. This equation,

$$\partial_t(\varphi P_R f_R) + \operatorname{div}(\overline{v}_R \varphi P_R f_R) + \partial_r(\overline{u}_R \varphi P_R f_R) = 0,$$

where $\overline{u}_R = (\overline{v \cdot \nabla R})_R$, $f_R = \langle \rho | R = r \rangle$, and $\overline{v}_R = \langle v\rho | R = r \rangle / f_R$, is suitable for simulation of pressure-driven flows with adsorption on the interface. Dependence of the properties of fluid flows in porous media on fractal properties of the media has been previously noted by Adler [1]. Here, in the following sections, the parameters of the PDCMC equation, specified by the intrinsic PDF P_R of the distance tracer R, are linked to the fractal properties of the porous media.

5. Fractality in porous media. The fluid/solid interface $\partial\Phi$ in porous media typically exhibits severe "ruggedness" which may, at least approximately, repeat itself on many different length scales. Such properties are usually identified as *self-similarity* or *fractality* [8, 21]. In the particular context considered, the fragment of $\partial\Phi$ enclosed by a sphere, or any other simple closed surface of fixed shape, with its center at an arbitrary point of the interface, appears as a complex spatial structure with numerous folds, ledges, and cavities which, when properly scaled, follow approximately the same ensemble of patterns as long as the observation window radius r is neither too small nor too large; see Figure 5.1. The last condition is understood as an asymptotic interval,

$$L_{\text{in}} \ll r \ll L_{\text{out}}, \tag{5.1}$$

whose endpoints, further referred to as the *inner* and *outer cutoffs*, are assumed to satisfy $L_{\text{in}} \ll L_{\text{out}}$. In the classical monofractal setting [8, Chapter 8], the pattern reproduction holds perfectly on all length scales, that is, $L_{\text{in}} = 0$ and $L_{\text{out}} = +\infty$. In a more realistic model of fractality [2, Chapter 12], the ensemble of patterns collapses on short length scales well below the inner cutoff—the interface runs out of

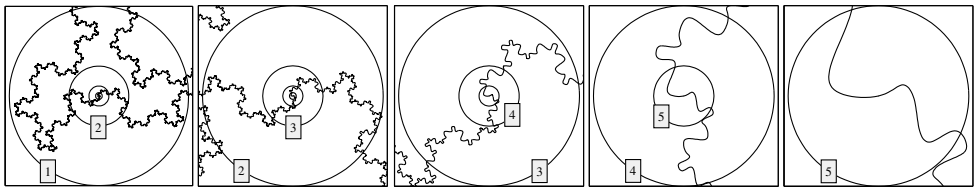

FIG. 5.1. *A fractal-like interface, observed through exponentially shrinking windows (left to right), stochastically repeats itself until the window radius reaches the inner cutoff* $L_{\rm in}$*, after which the surface gradually reveals its flat parts.*

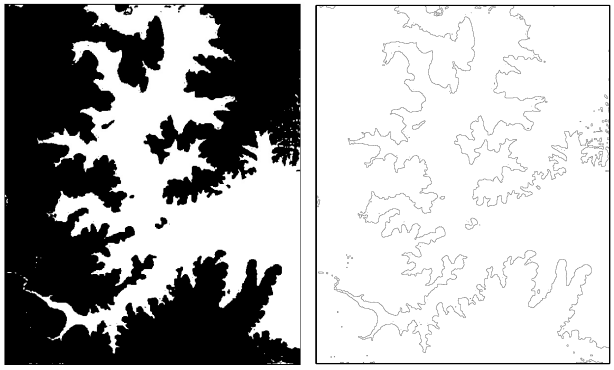

FIG. 5.2. *An illustration of a natural porous medium with fractal properties (left): the fluid phase (white) is lake Wivenhoe, Queensland, Australia, and the solid matrix (black) is the surrounding land. The interface is the shoreline (right). The pictures are produced by digital processing of satellite images from Imagery*©*2008 TerraMetrics, Map data*©*2008 MapData Sciences Pty Ltd, PSMA, and Google Maps.*

complexity, so that its fragments of linear size $r \ll L_{\rm in}$ are almost flat as if they were those of a plane. The outer cutoff, at the opposite extreme, quantifies the localness of the fractality—a small fragment of the interface is similar only to larger fragments whose size is bounded by $L_{\rm out}$, but not to the whole interface. Beyond $L_{\rm out}$, the local self-similarity is distorted by details of large-scale interaction of the porous medium with the environment which may vary from one sample to another without statistical stability. Further generalization towards real-world objects is the multifractal paradigm [30], where the ensemble of patterns slowly changes with r ranging over the interval in (5.1). We will, however, restrict our attention to the monofractal scenario, with the asymptotic interval of (5.1) describing the *monofractality range*.

The above considerations are also illustrated by lake shorelines in Figure 5.2, an example of the interface in a natural porous medium with fractal properties. Although the fragment of the lake system is ~ 10 km in size, similarly shaped pores may be massively observed in the surrounding rocks on microscopic scales. At the same time, the figure shows a gradual simplification of the shorelines when moving to the northern part of the region and suggests that the outer cutoff in the example can be estimated roughly as $L_{\rm out} \sim 1$ km. These pictures also demonstrate that, in general, if the interface of a porous medium exhibits local self-similarity in a wide range of spatial scales which amount to a significant portion of the volume, it is, in fact, hard to decouple the well-developed fractality of the interface from that of the set occupied

by the fluid phase. Moreover, the *interface fractality* can coexist with another type of self-similarity where the fluid phase set is composed of similar regions which are attached to each other as nodes in a complex spatial network. The interplay between the interface and network scenarios of fractality will be considered in sections 9 and 10.

The fractality in porous media may be qualitatively explained as a result of the very process of their formation. The fact that fractal properties of porous media are strongly influenced by weathering processes finds experimental evidence in materials science [5, pp. 50–51] and petrography [27, pp. 615–618]. Insignificant cracks at the surface of solid rocks gradually deepen in the course of long-term erosion and weathering that produces pores with increased surface area. Their large-scale exterior may still retain traces of the initial conditions but gradually ceases to be the main scene of interaction with the surroundings. The enlarged internal surface creates a far broader front for physical and chemical "intrusion" of the environment. The overwhelming portion of the front becomes isolated from immediate contact with the surroundings, making the effect of the outside geometric details fade. Instead, the network of pores plays the role of a unified intermediary for the exchange of heat with the environment and delivery of liquid and gaseous reactants from the outside. Different small parts of the surface are exposed to the same physicochemical process which repeats itself almost independently all over the surface in multiple parallel copies feeding on the common supply. The latter creates competition and hierarchy, which lead to establishment of statistically stable patterns reproduced in different fragments of the surface. It is probably at this stage of formation that the porous medium acquires well-developed fractal properties. The fractality development stage, however, is consuming and cannot last forever—the internal surface becomes so huge that its further evolution slows down because, due to the limited mass transmission capacity of the pores, the supply rate suffices only for the surface reactions to run at a decreased pace. Note that reproducing or at least mimicking the formation process is the main idea of *process models* [13, pp. 353–355] for computer simulation of porous media.

6. Distance tracer and contact dimension. To quantify the fractal properties of the interface discussed above, consider a scalar field R defined as the shortest Euclidean distance of a point x to the solid matrix by

$$R(x) := \min_{y \in \Phi^{\mathrm{C}}} |x - y|. \tag{6.1}$$

Equivalently, $R(x)$ is the largest radius r of an open ball $B(x, r)$ centered at x and contained entirely by the fluid phase. Its boundary

$$\Sigma(x) := \partial B(x, R(x)) \tag{6.2}$$

is called the *contact sphere*; see Figure 6.1. The function R will be referred to as the *distance tracer*. If the fluid phase indicator function β in (3.1) is a homogeneous random field, then so is R. Its value $R(x)$ at a fixed but otherwise arbitrary point x is a nonnegative random variable which is positive with probability $\mathsf{P}(R(x) > 0) = \varphi$, defined by (3.2), and vanishes with $\mathsf{P}(R(x) = 0) = 1 - \varphi$. Thus, the one-point distribution of the random field R is completely specified by the porosity φ and by the PDF $P_R(r) := \partial_r F_R(r)$, where

$$F_R(r) := \mathsf{P}(R(x) < r \mid x \in \Phi) = \mathsf{P}(0 < R(x) < r)/\varphi \tag{6.3}$$

is the conditional cumulative distribution function of $R(x)$, provided that the latter

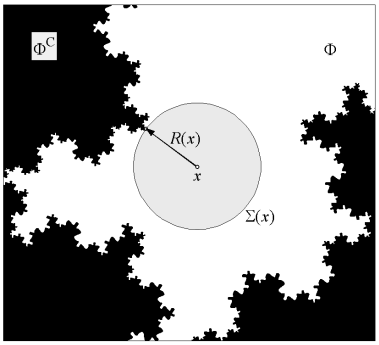

FIG. 6.1. *A cross section of the contact sphere $\Sigma(x)$ with center x in the fluid phase Φ. Its radius $R(x)$ is the shortest distance to the solid matrix Φ^{C}.*

is positive. Although P_R is defined using the ensemble probability measure, it will be referred to as the *intrinsic* PDF of R in order to emphasize its association with the fluid phase via the conditioning in (6.3). Since $F_R(0) = 0$ and $F_R(+\infty) = 1$, the intrinsic PDF satisfies the normalization condition $\int_0^{+\infty} P_R(r)\mathrm{d}r = 1$. We restrict our attention to the homogeneous case for simplicity, though the treatment is extendible to the general nonhomogeneous setting where P_R and F_R depend also on x. Following [13, p. 330], we call F_R the *contact distribution function*. If the distance tracer is ergodic, then the probability $F_R(r)$ in (6.3) coincides with the intrinsic volume fraction of a near-interface layer of thickness r,

$$\Lambda(r) := \bigcup_{y\in\partial\Phi} B(y,r) \cap \Phi \tag{6.4}$$

formed by those points in the fluid phase whose distance to the solid matrix is less than r. On one side, the layer is attached to the solid matrix, while the other lies in the fluid phase. The area of the latter surface per unit volume of the fluid phase is equal to $P_R(r)$, which clarifies the geometric meaning of the intrinsic PDF. Thus,

$$\sigma := \lim_{r\to 0+} P_R(r) \tag{6.5}$$

is the interface area per unit volume of the fluid phase. The conditional probability distribution of the distance field R within the layer $\Lambda(r)$ is described by the function

$$\theta_r(s) := \mathsf{P}(0 < R(x) < sr)/\mathsf{P}(0 < R(x) < r) = F_R(sr)/F_R(r), \tag{6.6}$$

where $0 < s \leqslant 1$ is the dimensionless scaling variable. Now, if the interface $\partial\Phi$ is locally self-similar as discussed in section 5, then, ignoring for the moment the leftmost restriction in (5.1), all the distances in the sublayer $\Lambda(sr)$ stochastically reproduce those in the layer $\Lambda(r)$ upon appropriate rescaling for small r, and hence $\theta_r(s)$ ceases to depend on r. The latter is understood as existence of a strictly positive continuous limit function $\theta(s) := \lim_{r\to 0+}\theta_r(s)$. Therefore, substituting the limit θ for θ_r on the left-hand side of (6.6) gives an asymptotic functional equation $F_R(sr) \sim \theta(s)F_R(r)$ as $r \to 0+$, which implies the exact functional equation $\theta(s)\theta(u) = \theta(su)$ whose solution is given by the power law $\theta(s) = s^b$ with exponent $b > 0$. Hence, the asymptotic behavior of the contact distribution function is

$$F_R(r) \sim \gamma r^b, \qquad r \to 0+, \tag{6.7}$$

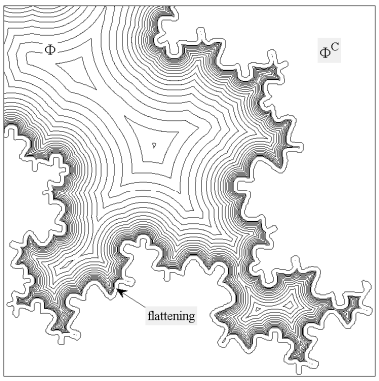

FIG. 6.2. *A cross section of isosurfaces of the distance tracer R for a porous medium with fractal properties on a truncated logarithmic scale of levels exceeding the inner cutoff $L_{\rm in}$. The flattening zone is the relatively thin fluid phase layer of thickness $\ll L_{\rm in}$ in the immediate vicinity of the interface.*

with a constant $\gamma > 0$. From the geometric meaning of F_R and (6.5), the exponent b is representable as

$$b := 1 - a, \tag{6.8}$$

where $0 < a < 1$ is interpreted as an *excess dimension* of the interface with respect to a flat surface. Indeed, if a were zero, then the intrinsic volume fraction of the layer $\Lambda(r)$ in (6.4) would be proportional to r for small values of r, and the coefficient γ in (6.7) would be equal to the interface area per unit volume of the fluid phase in (6.5). However, since $a > 0$, then the intrinsic volume fraction of $\Lambda(r)$ vanishes at a slower sublinear rate $\propto r^{1-a}$ as $r \to 0+$, a manifestation of the Gabriel's horn effect [10] associated with surfaces of infinite area which enclose finite volumes. Hence, employing the Minkowski–Bouligand variant of fractal dimension [7, section II.A], the fractal properties of the interface $\partial\Phi$ can be quantified by its *contact dimension* defined as

$$\mu := 3 - \lim_{r\to 0+} \log_r F_R(r) = 2 + a \tag{6.9}$$

in accordance with (6.7) and (6.8). An alternative assumption, which is slightly stronger than, though conforming with, (6.7), is

$$P_R(r) \sim b\gamma r^{-a}, \qquad r \to 0+. \tag{6.10}$$

Note, however, that in view of the qualitative discussions in section 5, the asymptotic behavior of the contact distribution function F_R and the related intrinsic PDF P_R, described by (6.7) and (6.10), as well as the limit in (6.9), should be understood as intermediate asymptotics [2] which manifest themselves only in the monofractality range specified by (5.1). For $r \ll L_{\rm in}$, the fractality collapses due to flattening of the interface on the short length scales, so that $P_R(r)$ achieves saturation and $F_R(r)$ becomes asymptotically linear in r; see Figures 6.2 and 6.3. The relative volume fraction of the flattening zone with respect to the intermediate monofractality layer can be estimated by the ratio

$$F_R(L_{\rm in})/F_R(L_{\rm out}) \sim (L_{\rm in}/L_{\rm out})^b \ll 1, \tag{6.11}$$

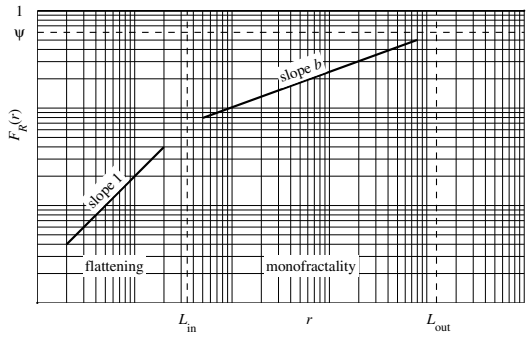

FIG. 6.3. *In the monofractality scenario, a typical log-log graph of the contact distribution function $F_R(r)$ of* (6.3) *has a linear asymptote with slope* 1 *in the flattening zone $r \ll L_{\rm in}$, and the intermediate power law asymptote with slope $b < 1$ from* (6.8) *in the monofractality range $L_{\rm in} \ll r \ll L_{\rm out}$. The threshold ψ is the intrinsic volume fraction of the intermediate monofractality layer of the fluid phase.*

obtained by formal extrapolation of the power law of (6.7) to the inner and outer cutoffs. Note that its negligibility is, in fact, a stronger condition than the assumption $L_{\rm in} \ll L_{\rm out}$ if the interface excess dimension a is close to 1. By similar reasoning,

$$\gamma \sim \psi L_{\rm out}^{-b}, \tag{6.12}$$

where ψ is the intrinsic volume fraction of the intermediate monofractality layer of the fluid phase which, in view of (6.11), satisfies

$$\psi \sim F_R(L_{\rm out}). \tag{6.13}$$

Accordingly, the interface area per unit volume of the fluid phase σ from (6.5) can be estimated as

$$\sigma \sim F_R(L_{\rm in})/L_{\rm in} \sim \gamma L_{\rm in}^{-a} \sim (L_{\rm out}/L_{\rm in})^a\, \psi/L_{\rm out}, \tag{6.14}$$

where use is also made of (6.8) and (6.12). The specific internal area, that is, the interface area per unit volume of the porous medium, is $\sigma\varphi$, where φ is the porosity given by (3.2).

Several comments on (6.14) are in order. If the porous medium exhibits well-developed fractal properties, then the quantity ψ in (6.13) is comparable with 1. While the volume-to-thickness ratio, calculated for the flattening zone, is a good estimate of the area σ, a similar ratio, $\psi/L_{\rm out}$, associated with the monofractality layer, severely underestimates σ, so that $(L_{\rm out}/L_{\rm in})^a$ on the right-hand side of (6.14) plays the role of a correcting factor whose significance increases with the interface contact dimension μ.

7. Diffusion tracer and first hitting time. As mentioned previously, of particular interest for our purposes are probabilistic interpretations related to stochastic models of diffusion as a main transport mechanism in small pores where it dominates over convection. In what follows, the ensemble average $\langle \cdot \mid \Phi \rangle$, conditioned on the fluid phase set, will be written as $\mathsf{E}(\cdot)$, the standard probability theoretic notation for the expectation. Consider a Brownian motion $x + \sqrt{D}\mathcal{W}(t)$ starting from a point x in the fluid phase Φ at time $t = 0$. Here, $\mathcal{W}$ is an independent three-dimensional

standard Wiener process,[1] that is, the simplest Markov diffusion in $\mathbb{R}^3$, and D is a *diffusion coefficient* whose particular value is specified below. This is a well-known model for erratic paths of a particle in a fluid at rest under random external forces which destroy directional preferences and dependence on the past history, making the motion isotropic and memoryless. Consider the first time

$$\tau(x) := \min\{t \geqslant 0 :\ x + \sqrt{D}\mathcal{W}(t) \in \Phi^{\mathrm{C}}\} \tag{7.1}$$

when the Brownian motion hits the solid matrix. For a given realization of the fluid phase set Φ, the *first hitting time* $\tau(x)$ is a random variable, whose conditional expectation

$$Z(x) := \mathsf{E}\tau(x) \tag{7.2}$$

satisfies the Poisson PDE

$$\Delta Z(x) = -2/D, \qquad x \in \Phi, \tag{7.3}$$

in the fluid phase and vanishes on the solid matrix, $Z|_{\Phi^{\mathrm{C}}} = 0$. Indeed, from the defining equation (7.2), the function Z, evaluated on a sample path of the Brownian motion $x + \sqrt{D}\mathcal{W}$ until the first hitting time and then stopped, behaves as a random countdown to the encounter with the solid matrix. Assuming this encounter unavoidable, so that $\tau(x)$ is finite with probability 1, and denoting $t \wedge \tau := \min(t, \tau(x))$, the random process $(t\wedge\tau)+Z(x+\sqrt{D}\mathcal{W}(t\wedge\tau))$ is a martingale [14, 28]. Its Itô differential on the time interval $0 \leqslant t \leqslant \tau(x)$ is

$$\mathrm{d}(Z(x + \sqrt{D}\mathcal{W}) + t) = \sqrt{D}\nabla Z \cdot \mathrm{d}\mathcal{W} + (D\Delta Z/2 + 1)\mathrm{d}t.$$

Since the martingale property implies that the drift term vanishes identically, hence (7.3) follows. This equation initializes the recurrent Poisson PDEs for higher moments of the first hitting time, considered in Appendix C using a different reasoning whose details can be found in [11]. Now, ascribing to the diffusion coefficient the value $D := 2D_0/W_0$, note that (7.3) reproduces the Poisson equation (4.14) near the interface, and hence its solution, which is assumed unique, asymptotically reproduces the diffusion tracer Z in the near-interface region.

Therefore, although Z was initially associated with the mass fraction of an ancillary species, (7.1) and (7.2) provide the diffusion tracer with another interpretation—as the average time needed for the Brownian motion to reach the solid matrix. In addition to rendering a temporal proximity of x to the solid phase, $Z(x)$ also quantifies the spatial distance. Indeed, consider the *first hitting point*

$$\eta(x) := x + \sqrt{D}\mathcal{W}(\tau(x)), \tag{7.4}$$

which, for any $x \in \Phi$, is a random vector with values in $\partial\Phi$. Applying the optional sampling theorem [25, 28] to the martingales[2] $\mathcal{W}(t)$ and $\mathcal{W}(t)\mathcal{W}(t)^{\mathrm{T}} - tI_3$ at the

[1] Recall that $\mathcal{W}$ is a strongly Markov Gaussian process with continuous sample paths $0 \leqslant t \mapsto \mathcal{W}(t) \in \mathbb{R}^3$ satisfying $\mathcal{W}(0) = 0$ and having zero mean $\mathsf{E}\mathcal{W}(t) = 0$ and covariance function $\mathsf{E}(\mathcal{W}(s)\mathcal{W}(t)^{\mathrm{T}}) = \min(s,t)I_3$, where $(\cdot)^{\mathrm{T}}$ is the transpose, all the vectors are organized as columns, and I_3 is the identity matrix of order 3.

[2] Indeed, $\mathsf{E}\left(\mathcal{W}(t)\mathcal{W}(t)^{\mathrm{T}} \mid \mathcal{W}_{[0,s]}\right) = \mathcal{W}(s)\mathcal{W}(s)^{\mathrm{T}} + (t-s)I_3$ for all $0 \leqslant s \leqslant t$ since the increment $\mathcal{W}(t) - \mathcal{W}(s)$ is independent of the past history $\mathcal{W}_{[0,s]}$ of $\mathcal{W}$ on the time interval $[0, s]$ and has zero mean and covariance matrix $(t-s)I_3$.

moment of time[3] $\tau(x)$ whereby their expected values are the same as at $t = 0$ when they both vanish, the conditional expectation and covariance matrix of $\eta(x)$ in (7.4) are $\mathsf{E}\eta(x) = x$ and $\mathsf{E}((\eta(x) - x)(\eta(x) - x)^{\mathrm{T}}) = DZ(x)I_3$. Hence, the variance of $\eta(x)$ is

$$\mathsf{E}(|\eta(x) - x|^2) = 3DZ(x). \tag{7.5}$$

Since $|\eta(x) - x|$ is not less than the shortest distance $R(x)$ from the point x to the solid matrix Φ^{C} defined by (6.1), then (7.5) implies a *distance-diffusion inequality*

$$R(x) \leqslant \sqrt{3DZ(x)}. \tag{7.6}$$

Thus, the diffusion tracer Z also provides an upper bound for the spatial proximity to the solid phase described by the distance tracer R. Furthermore, $\sqrt{DZ(x)}$ is a characteristic linear size of that part of the interface $\partial\Phi$ which is "most accessible" to a Brownian motion from x in the fluid phase. Indeed, combining Chebyshev's inequality [29] with (7.5) yields

$$\mathsf{P}(|\eta(x) - x| > w\sqrt{DZ(x)} \mid \Phi) \leqslant \mathsf{E}(|\eta(x) - x|^2)/(DZ(x)w^2) = 3/w^2. \tag{7.7}$$

Hence, for a large dimensionless parameter $w \gg 1$, the probability on the left-hand side of (7.7) is negligibly small, so that the distribution of the first hitting point $\eta(x)$ (that is, the harmonic measure [25] associated with Φ) is mainly concentrated on $\partial\Phi \cap B(x, w\sqrt{DZ(x)})$. It also seems reasonable to conjecture that $\sqrt{DZ(x)}$ qualitatively characterizes the linear size of that part of $\partial\Phi$ which noticeably influences $Z(x)$, so that the latter is slightly sensitive to small perturbations of the interface beyond that distance from x.

Thus, although the boundary of the connected component of Φ which contains x is reachable for the Brownian motion $x + \sqrt{D}\mathcal{W}$ even if this component is unbounded, the dependence of $Z(x)$ on the geometry of the interface is, to a certain extent, local. This *quasi-localness* extends in a *cascade* manner to z-isosurfaces of Z and determines the rate of their gradual smoothing as the level z monotonically increases. Indeed, for any given $z > 0$, the isosurface $Z = z$ plays the same role for the superlevel set $Z > z$ as $\partial\Phi$ does for Φ in the sense that the biased tracer $Z - z$ vanishes at this isosurface and satisfies the same Poisson PDE. In particular, for any $z_1 > z_2 > 0$, the average time needed for the Brownian motion $x + \sqrt{D}\mathcal{W}$ to reach the isosurface $Z = z_2$ from a fixed but otherwise arbitrary point x of the isosurface $Z(x) = z_1$ is given by $\mathsf{E}\min\{t \geqslant 0 : Z(x + \sqrt{D}\mathcal{W}(t)) = z_2\} = z_1 - z_2$. In section 11, we will utilize this cascade idea in a different manner, employing the harmonic measures associated with the superlevel and sublevel sets of the distance tracer.

8. Integral relationships. An additional insight into the relationship between the distance and diffusion tracers is provided by the integral equation

$$Z(x) = r^2/(3D) + \frac{1}{4\pi}\int_{|s|=1} Z(x + rs)\mathrm{d}s, \qquad 0 \leqslant r \leqslant R(x), \tag{8.1}$$

which is also valid, though trivial, with $r = 0$, in the solid matrix. Here, the normalized surface integral is the mean value of the diffusion tracer Z on the sphere

[3]The random variable $\tau(x)$ in (7.1) is a stopping time [28] with respect to the process $\mathcal{W}$ in the sense that for any $t \geqslant 0$, the random event $\{\tau(x) \leqslant t\}$, and hence its complement $\{\tau(x) > t\}$, is completely determined by the past history of $\mathcal{W}$ on the interval $[0, t]$, so that the behavior of $\mathcal{W}$ beyond the time horizon t is irrelevant for deciding whether the event has happened or not.

$\partial B(x,r)$ which is enclosed by the contact sphere $\Sigma(x)$ defined by (6.2). This integral equation can also be written using the more conventional volume, rather than surface, averaging. Indeed, (8.1) implies that for an isotropic kernel function $K(y) := K(|y|)$, with K of bounded support and normalized to $4\pi\int_0^{+\infty} K(r)r^2\mathrm{d}r = 1$, the K-weighted moving average of Z, defined by (A.1) of Appendix A, satisfies $Z(x) = 4\pi\int_0^{+\infty} K(r)r^4\mathrm{d}r/(3D) + \langle Z\rangle_K(x)$ at those points x where $R(x)$ is not less than the support radius of K (for such points, $\langle Z\rangle_K$ is an intrinsic volume average). Extending (8.1) in a different direction,

$$Z(x) = (r^2 - |x-c|^2)/(3D) + \int_{\partial B(c,r)} \frac{r^2 - |x-c|^2}{4\pi r|s-x|^3} Z(s)\mathrm{d}s, \qquad x \in B(c,r), \tag{8.2}$$

for any ball $B(c,r)$ contained by Φ. Here, the fist term is the solution of the Poisson PDE of (7.3) in the ball with zero boundary condition, whose probabilistic interpretation is as follows. Since the sphere $\partial B(c,r)$ separates the point x in the fluid phase from the solid matrix, then, recalling (7.1), the time interval $[0,\tau(x)]$ is split into two intervals $[0,\tau_{c,r}(x)]$ and $[\tau_{c,r}(x),\tau(x)]$, where

$$\tau_{c,r}(x) := \min\{t \geqslant 0 :\ |x + \sqrt{D}\mathcal{W}(t) - c| = r\} \tag{8.3}$$

is the first time when the Brownian motion $x+\sqrt{D}\mathcal{W}$ hits the sphere, which precedes the collision with the solid matrix. For a given realization of the fluid phase set Φ, the expected value of the first hitting time $\tau_{c,r}(x)$ is

$$\mathsf{E}\tau_{c,r}(x) = (r^2 - |x-c|^2)/(3D), \tag{8.4}$$

which can be obtained directly by solving the Poisson PDE among quadratic polynomials vanishing on the sphere; see also [25, p. 125]. The same ansatz class of functions is suitable for more complex quadratic surfaces, for example, ellipsoids, though spheres are preferable here due to the isotropy of $\mathcal{W}$. Note that the quadraticity of the right-hand side of (8.4) with respect to r and $|x-c|$ is closely related to the invariance of the standard Wiener process $\mathcal{W}$ in distribution under the spatiotemporal rescaling $\mathcal{W}(t) \mapsto u\mathcal{W}(t/u^2)$ for any $u \neq 0$ (which is responsible for the stochastic self-similarity of $\mathcal{W}$).

The surface integral in (8.2) is the harmonic function described by the Poisson integral formula [31, section 29 in Chapter V] for the appropriate Dirichlet problem with boundary value Z. The Poisson kernel, as a function of s, is the PDF of the first hitting point

$$\eta_{c,r}(x) := x + \sqrt{D}\mathcal{W}(\tau_{c,r}(x)) \tag{8.5}$$

associated with (8.3). This integral equation is closely related to the strong Markov property [25] of $\mathcal{W}$. Indeed, the probability distribution of the random variable $\tau(x) - \tau_{c,r}(x)$, conditioned on the history of the Brownian motion $x + \sqrt{D}\mathcal{W}$ on the time interval $[0,\tau_{c,r}(x)]$, depends only on its last value $\eta_{c,r}(x)$ as if the latter were the initial position, so that, recalling (7.2),

$$\mathsf{E}\left(\tau(x) - \tau_{c,r}(x) \mid \mathcal{W}_{[0,\tau_{c,r}(x)]}\right) = \mathsf{E}(\tau(x) - \tau_{c,r}(x) \mid \eta_{c,r}(x)) = Z(\eta_{c,r}(x)). \tag{8.6}$$

Therefore, combining (8.4) and (8.6) with the tower property of iterated conditional expectations [29] yields the relation

$$Z(x) = \mathsf{E}\tau_{c,r}(x) + \mathsf{E}\mathsf{E}(\tau(x) - \tau_{c,r}(x) \mid \eta_{c,r}(x)) = (r^2 - |x-c|^2)/(3D) + \mathsf{E}Z(\eta_{c,r}(x)).$$

Its right-hand side coincides with that of (8.2) since the PDF of $\eta_{c,r}(x)$ in (8.5) is given by the Poisson kernel describing the harmonic measure associated with the ball $B(c,r)$.

As mentioned above, (8.1) is a particular case of (8.2) with $c := x$. In turn, the distance-diffusion inequality of (7.6) can be obtained from (8.1), which, by putting $r := R(x)$, reads

$$Z(x) = R(x)^2/(3D) + \frac{1}{4\pi}\int_{|s|=1} Z(x + R(x)s)\mathrm{d}s \tag{8.7}$$

and, omitting the nonnegative integral, implies

$$Z(x) \geqslant R(x)^2/(3D). \tag{8.8}$$

The lower bound for the diffusion tracer provided by (8.8) can be successively improved by iterating the affine operator on the right-hand side of (8.7) and subsequently discarding the surface integral of Z. For example, the next iteration yields

$$Z(x) \geqslant \frac{1}{3D}\left(R(x)^2 + \frac{1}{4\pi}\int_{|s|=1} R(x + R(x)s)^2\mathrm{d}s\right).$$

Repeating the iterations infinitely, without truncation, as in the spherical sweeping procedure of [26, pp. 223–224], gives

$$Z(x) = \frac{1}{3D}\sum_{k=0}^{+\infty} \mathsf{E}(R(\xi_k)^2). \tag{8.9}$$

Here, for a given realization of Φ, the random vectors $\xi_0, \xi_1, \ldots$ form a Markov sequence starting from $\xi_0 := x$ and such that the transition probability distribution from ξ_k to ξ_{k+1} is the uniform distribution over the contact sphere $\Sigma(\xi_k)$ centered at ξ_k. The right-hand side of (8.9) is a probabilistic form of the Neumann series [31, section 17 in Chapter IV] for the Fredholm integral equation of the second kind in (8.7), where the normalized surface integral describes a linear operator, acting on Z, whose spectral radius does not exceed 1. An alternative way to refine the distance-diffusion inequality of (8.8) is described in Appendix D and employs an additional geometric construct in the context of (8.2). Another byproduct of the latter integral equation is a *maximum localization principle*, established in Appendix E.

9. Basins of attraction to local maxima. By the maximum localization principle of Appendix E, if a ball $B(c,r)$ is contained by Φ and the oscillation of the diffusion tracer Z on the sphere $\partial B(c,r)$ is less than $r^2/(3D)$, then Z has at least one local maximum inside the sphere. As we will see below, local maxima of Z are convenient reference points which allow Φ to be split into "chunks" of the fluid phase. To this end, consider an ancillary dynamical system with phase space Φ governed by the ordinary differential equation (ODE)

$$\dot{x} = \nabla Z(x). \tag{9.1}$$

Its phase trajectories are normal to isosurfaces of Z and coincide with the heatlines mentioned in section 4 except that they are oriented oppositely. By (7.3) and Liouville's theorem, (9.1) shrinks the phase volume by the exponential law $\exp(-2t/D)$

in time t. Furthermore, since $\dot{Z} = |\nabla Z|^2$, the function Z is strictly increasing along the trajectories, thereby playing the role of a Lyapunov function. Thus, the strong local maxima of the diffusion tracer Z (where, in addition to the necessary condition $\nabla Z = 0$, the Hessian matrix Z'' is negative definite) are asymptotically stable equilibria of (9.1). Assuming a typical situation where they exhaust all local maxima of Z, these points form a countable subset X of the fluid phase. Discarding subsets of volume zero, Φ is partitioned into *basins of attraction* $\Psi(x_*)$ of the local maxima $x_* \in X$. More precisely, $\Psi(x_*)$ is formed by points of all those phase trajectories of the ODE which converge to x_*, including x_* itself. The local maximum value of the diffusion tracer $Z(x_*)$ is, in fact, global within the unique basin of attraction $\Psi(x_*)$ which contains a given point $x \in \Phi$, that is,

$$Z_*(x) := Z(x_*) = \max_{y \in \Psi(x_*)} Z(y), \qquad x \in \Psi(x_*). \tag{9.2}$$

The piecewise constant function $Z_*(x)$ satisfies $Z_*(x) \geqslant Z(x)$ and, unlike $Z(x)$, describes the largeness of the pore to which x belongs, rather than the proximity of this point to the solid matrix. Similarly, the physical size of the basin of attraction $\Psi(x_*)$ can be quantified by

$$L(x) := R(x_*), \tag{9.3}$$

which is also a piecewise constant function of x. Therefore, as the contact sphere $\Sigma(x_*)$ traverses the "outskirts" of the domain $\Psi(x_*)$, then in view of (8.1) taking the form

$$Z_*(x) = L(x)^2/(3D) + \int_{\Sigma(x_*)} Z(s)\mathrm{d}s/(4\pi L(x)^2), \tag{9.4}$$

the first quadratic term is to play a leading part in the conditional distribution of Z_* with respect to L. To formulate it more precisely as a scaling hypothesis, additional remarks on the geometry of the basins of attraction are in order. The boundary of $\Psi(x_*)$ can be partitioned into two subsets,

$$\partial\Psi(x_*) = (\partial\Phi \cap \partial\Psi(x_*)) \sqcup (\Phi \cap \partial\Psi(x_*)), \tag{9.5}$$

with $\sqcup$ the union of disjoint sets, the first of which is a subset of the fluid/solid interface $\partial\Phi$ and the second is formed by *separatrix manifolds* that are contained by the fluid phase and shared by the boundaries of adjacent basins of attraction; see Figure 9.1. The phase trajectories of (9.1), started close to the separatrix but on opposite sides from it, are attracted by different local maxima of Z. As Figure 9.2 suggests, each of the separatrices of the gradient flow contains an unstable saddle-type equilibrium where the Hessian matrix Z'' has two negative eigenvalues and one positive, with the appropriate eigenvector normal to the separatrix. Such an equilibrium plays the role of a scattering center which gathers phase trajectories, started at points of the interface $\partial\Phi$ close to the separatrix, and then scatters them in two opposite directions, specified by the unstable eigenvector, along two "highways" leading to the local maxima of Z. At noncritical points, where $\nabla Z \neq 0$, the separatrices are normal to isosurfaces of Z, that is, tangential to the gradient field ∇Z, so that the flux of ∇Z across any subset of the separatrix is zero. Therefore, the basins of attraction can be regarded as nodes of a complex spatial network which are geometrically linked through separatrices. At the same time, the separatrices insulate the nodes from each other in the sense of the

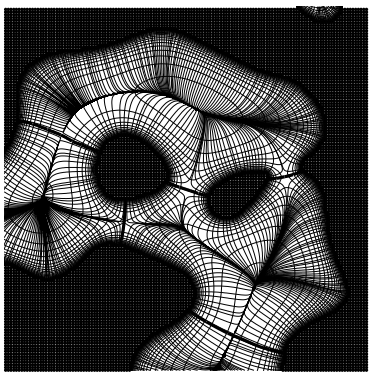

FIG. 9.1. *An illustration of the phase portrait of* (9.1). *Also shown are the isolines of the diffusion tracer* Z *and the separatrices (bold curves) of the basins of attraction of local maxima.*

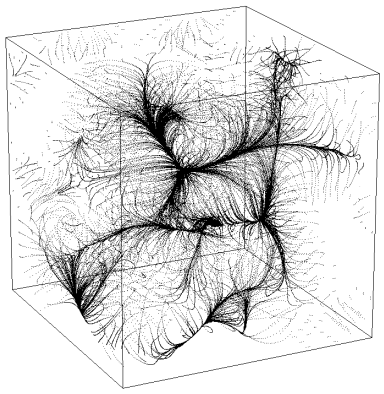

FIG. 9.2. *A typical phase portrait of* (9.1) *in three dimensions.*

gradient flow ∇Z, so that in every basin of attraction, the diffusion tracer solves an autonomous mixed boundary value problem for the Poisson PDE in (7.3),

$$\Delta Z(x) = -2/D, \quad x \in \Psi(x_*), \quad Z|_{\partial\Phi\cap\partial\Psi(x_*)} = 0, \quad \partial_n Z|_{\Phi\cap\partial\Psi(x_*)} = 0, \tag{9.6}$$

where $\partial_n Z := n \cdot \nabla Z$ is the normal derivative of Z across the separatrix. Note, however, that the problems in (9.6) are autonomous only a posteriori since the domains, where they are considered, are determined in terms of Z found in advance in the whole fluid phase set.

Now, if the network of basins of attraction to local maxima of Z exhibits fractality in the sense of similarity of its nodes, including the interface-separatrix partitions of their boundaries in (9.5), then, recalling (9.2), (9.3), and (9.4), it seems reasonable to assume the following *network distance-diffusion scaling* for the conditional PDF of $Z_*(x)$ for a given positive level $L(x) = \ell$:

$$w^2 P_{Z_*|L}(w^2 z_* \mid w\ell) = P_{Z_*|L}(z_* \mid \ell)$$

for all $0 < \ell \leqslant \sqrt{3Dz_*}$ and any $w > 0$, where the leftmost factor w^2 ensures the normalization condition $\int_{\ell^2/(3D)}^{+\infty} P_{Z_*|L}(z_* \mid \ell)\mathrm{d}z_* = 1$. This assumption is equivalent

to saying that the dimensionless random variable

$$Q(x) := DZ_*(x)/L(x)^2, \tag{9.7}$$

which is well-defined and piecewise constant for $x \in \Phi$, is conditionally independent of $L(x)$, and hence

$$P_{Z_*|L}(z_* \mid \ell) = D\ell^{-2} P_Q(Dz_*/\ell^2), \tag{9.8}$$

where P_Q is the intrinsic PDF of $Q(x)$ satisfying $\int_{1/3}^{+\infty} P_Q(q)\mathrm{d}q = 1$. The rationale behind this scaling is twofold. First, for the solution of the Poisson PDE $\Delta f =$ const with constant right-hand side in a domain $M = M_1 \sqcup M_2$ and mixed boundary conditions $f|_{\partial M_1} = 0$ and $\partial_n f|_{\partial M_2} = 0$, the homothety $M \mapsto sM$, appropriately extended to M_1 and M_2, with nonzero similitude ratio s implies the scaling $f(x) \mapsto s^2 f(x/s)$, and a similar scaling holds for compositions of the homothety with rigid motions (translations, reflections, and rotations) of the physical space. The property is closely related to the spatiotemporal scale-invariance of the standard Wiener process mentioned in section 8. Second, the network self-similarity allows the nodes (the basins of attraction to local maxima of Z) to be regarded as a random assemblage of motifs M which are reproduced on different length scales. Hence, if $\Psi(x_1)$ is an s-scaled copy of $\Psi(x_2)$ up to a rigid motion, then the diffusion tracer Z is reproduced within $\Psi(x_1)$ as the s^2-scaling of itself from $\Psi(x_2)$; see, for example, Figure 9.3.

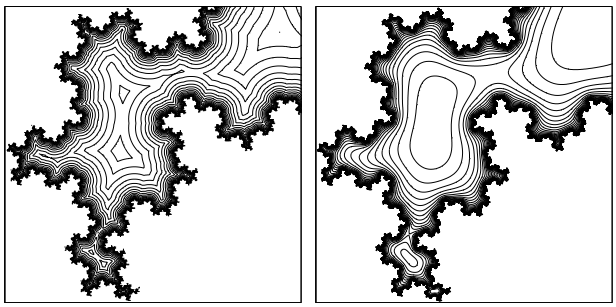

FIG. 9.3. *A cross section of isosurfaces of the distance tracer R (left) and the diffusion tracer Z (right), each with its own logarithmic level scale, for a porous medium with fractal properties.*

10. Isolation of relative scales. The largeness of the basin of attraction $\Psi(x_*)$ to a local maximum of Z, containing a given point x of the fluid phase, is quantified by $L(x)$ and $Z_*(x)$ from (9.3) and (9.2), while the relative proximity of the point to the fluid/solid interface is described by the ratios

$$U(x) := R(x)/L(x), \qquad V(x) := Z(x)/Z_*(x), \tag{10.1}$$

referred to as the *relative* distance and diffusion tracers. The conditional joint distribution of these four random variables, provided that $x \in \Phi$, can be used to deduce the intrinsic PDF of the diffusion tracer Z. To this end, in addition to the network distance-diffusion scaling hypothesis of section 9 on the independence of Q in (9.7) and L, we assume that the pairs of random variables (U, V) and (L, Z_*) are also independent, so that the relative scales are stochastically "isolated" from the "pore

largeness" variables. These two assumptions are equivalent to the factorization of the intrinsic joint PDF of the random variables L, R, Z_*, and Z as

$$P_{Z,Z_*,R,L}(z,z_*,r,\ell) = DP_{V|U}(z/z_* \mid r/\ell)\, P_U(r/\ell)\, P_Q(Dz_*/\ell^2)\, P_L(\ell)/(z_*\ell^3). \tag{10.2}$$

Here, the conditional PDF $P_{V|U}(v \mid u)$ vanishes for $v < u^2$, which, in combination with $P_Q(q) = 0$ for $q < 1/3$, ensures that the PDF $P_{Z,Z_*,R,L}$ in (10.2) can only be nonzero for $z \geqslant r^2/(3D)$ and $z_* \geqslant \ell^2/(3D)$, in conformance with the distance-diffusion inequality of (8.8). Hence, the intrinsic PDF of Z is computed as

$$P_Z(z) = \int_z^{+\infty} z_*^{-1} P_V(z/z_*) P_{Z_*}(z_*) \mathrm{d}z_*, \tag{10.3}$$

where the integral is the convolution of the PDFs P_V and P_{Z_*} on the positive half-axis $(0,+\infty)$ considered as a multiplicative group with Haar measure $u^{-1}\mathrm{d}u = \mathrm{d}\ln u$, and

$$P_V(v) = \int_0^{\sqrt{v}} P_{V|U}(v \mid u) P_U(u) \mathrm{d}u, \tag{10.4}$$

$$P_{Z_*}(z_*) = D \int_0^{\sqrt{3Dz_*}} \ell^{-2} P_Q(Dz_*/\ell^2) P_L(\ell) \mathrm{d}\ell. \tag{10.5}$$

Therefore, under the assumptions of network distance-diffusion scaling and isolation of relative scales, P_Z is completely specified by $P_{V|U}$, P_U, P_Q, and P_L. As a first approximation, which is, nevertheless, fairly accurate for nearly spherical nodes (see Appendix F), the random variable Q is close to $1/3$, so that the PDF of Z_* can be approximated by that of $L^2/(3D)$,

$$P_{Z_*}(z_*) \approx \frac{1}{2}\sqrt{3D/z_*}\, P_L(\sqrt{3Dz_*}), \tag{10.6}$$

thereby discarding the need for detailed knowledge of P_Q required by (10.5). Postponing the discussion of the conditional PDF $P_{V|U}$ until section 11, we consider P_U and P_L. From the independence of U and L, assumed above, the intrinsic PDF of the distance tracer is representable by a convolution

$$P_R(r) = \int_0^{+\infty} \ell^{-1} P_U(r/\ell) P_L(\ell) \mathrm{d}\ell, \tag{10.7}$$

similar to (10.3). This representation allows the power law for P_R in (6.10) to be related with that of P_L. As a rule of thumb, let L be bounded by the inner and outer cutoffs discussed in sections 5 and 6 and have PDF

$$P_L(\ell) := (1-\alpha)\ell^{-\alpha} \big/ \left(L_{\mathrm{out}}^{1-\alpha} - L_{\mathrm{in}}^{1-\alpha}\right), \qquad L_{\mathrm{in}} < \ell < L_{\mathrm{out}}, \tag{10.8}$$

which vanishes beyond the interval, so that too small and too large pores are prohibitively atypical. Here, $0 < \alpha < 1$ quantifies the network fractality of the porous medium in addition to the previously introduced interface excess dimension a. Application of (10.7) to the truncated power law of (10.8), where $L_{\mathrm{in}}^{1-\alpha}$ can be removed from the denominator without severe loss of accuracy in view of $L_{\mathrm{in}} \ll L_{\mathrm{out}}$, gives

$$P_R(r) = \int_{r/L_{\mathrm{in}}}^{r/L_{\mathrm{out}}} u^{-1} P_U(u) P_L(r/u) \mathrm{d}u \sim (1-\alpha) L_{\mathrm{out}}^{\alpha-1} \int_0^{+\infty} P_U(u) u^{\alpha-1} \mathrm{d}u\, r^{-\alpha}. \tag{10.9}$$

This asymptotic relation is valid in the monofractality range described by (5.1) if the rightmost integral is finite. In this case, the asymptotic behavior of P_R matches the power law in (6.10) only if $\alpha = a$. The integrability can be corrupted by the behavior of $P_U(u)$ only as $u \to 0+$, since $P_U(u)$ decays fast for $u \gg 1$. The latter follows from the qualitative observation that, in a typical situation, $L(x)$ is close to $\max_{x\in\Psi(x_*)} R(x)$ by the order of magnitude, and so, with an overwhelming probability, the ratio U in (10.1) does not exceed 1. In particular, the integrability condition is violated if $P_U(u)$ obeys asymptotically, for small u, the power law $u^{-\omega}$ with $\alpha < \omega < 1$. By describing this last scenario by an ansatz PDF

$$P_U(u) := (1-\omega)u^{-\omega}, \qquad 0 < u < 1, \tag{10.10}$$

which vanishes beyond the unit interval, it follows that (10.7) predicts a different asymptotic behavior

$$P_R(r) = (1-\omega)r^{-\omega}\int_r^{L_{\text{out}}} \ell^{\omega-1}P_L(\ell)\mathrm{d}\ell \sim (1-\alpha)(1-\omega)L_{\text{out}}^{\omega-1}r^{-\omega}/(\omega-\alpha) \tag{10.11}$$

in the monofractality range. Although the specific form of P_L from (10.8) influences the coefficient on the right-hand side of (10.11), the power law $r^{-\omega}$ itself remains valid to the extent that the multiplier ℓ^ω tempers the growth of $P_L(\ell)$ as ℓ approaches the inner cutoff. In this case, the conformance with (6.10) is achieved only if $\omega = a$.

As (10.9) and (10.11) suggest, in the competition of the PDFs P_L and P_U for the domination of either network or interface scenarios of fractality in the asymptotic behavior of P_R, the latter inherits the power law of the PDF whose exponent is greater by the absolute value. Moreover, the winner suppresses the effect of a specific shape of the other PDF. In what follows, we will restrict our attention to the case

$$\alpha < \omega = a, \tag{10.12}$$

where the network fractality is weaker than the interface fractality, and P_U follows the power law with the same exponent as P_R.

11. Lognormal cascade hypothesis. Since the functions L and Z_* are both constant on every basin of attraction $\Psi(x_*)$ to a local maximum of Z, the fields U and V defined by (10.1) inherit appropriately scaled properties of the distance and diffusion tracers R and Z, respectively. In particular, recalling (9.7), the relative diffusion tracer V satisfies the Poisson PDE

$$\widetilde{\Delta}V(x) = -2/Q(x), \qquad x \in \Psi(x_*), \tag{11.1}$$

and has local maxima at the same points as Z. Here, $\widetilde{\Delta} := (L\widetilde{\nabla})^2$ is the Laplacian in the "relative" spatial vector $\widetilde{x} := (x - x_*)/L$ in terms of which U measures the Euclidean distance to the solid matrix. Although V is discontinuous at separatrices between adjacent basins of attraction with different values of Z_*, the flux of $\widetilde{\nabla}V$ across any subset of the separatrices is zero. In the region where the relative tracers satisfy

$$U^2 \ll V \ll 1, \tag{11.2}$$

the right-hand side of (11.1), depending on the large-scale structure of the basin of attraction and its surroundings, becomes irrelevant, so that V conditioned on U is mainly driven by the flux of $\widetilde{\nabla}V$ across the isosurfaces of U rather than by the

source term of the Poisson equation. Therefore, in the region specified by (11.2), the relative diffusion tracer V behaves like a harmonic function. Hence, for two positive levels $u_1 < u_2 \ll 1$, the restriction $V|_{U=u_2}$ of V to the isosurface $U = u_2$ can be approximated by the average of $V|_{U=u_1}$ over the harmonic measure associated with the superlevel set of the relative distance tracer $U > u_1$. Alternatively, $V|_{u_1}$ can be approximated by

$$V|_{u_1} \approx H_{u_1,u_2} V|_{U=u_2}, \tag{11.3}$$

that is, by the image of $V|_{U=u_2}$ under the action of a linear operator H_{u_1,u_2}. The latter is generated by the harmonic measure associated with the sublevel set $0 < U < u_2$ whose boundary consists of the isosurface $U = u_2$ and the fluid/solid interface where V vanishes. The partial "loss" of the harmonic measure at the interface makes the operator H_{u_1,u_2} a contraction with respect to the supremum norm, though $H_{u,u}$, obtained in the limit as $u_1 \to u_2 = u$, is the identity map. Furthermore, the operators satisfy a semigroup property

$$H_{u_1,u_3} = H_{u_1,u_2} H_{u_2,u_3} \tag{11.4}$$

for $u_1 < u_2 < u_3$. Now, assume that, in terms of the conditional distribution of V with respect to U, the way (11.3) manifests itself in the passage from $U = u_2$ to a smaller scale $U = u_1 < u_2$ is equivalent to multiplying V by an independent random variable.

The above considerations provide a heuristic rationale for analogy with the lognormal hypothesis on the energy cascade through eddies of different length scales known in the statistical theory of turbulence [19]. The resulting multiplicative cascade leads to the intrinsic conditional PDF $P_{V|U}$ of the relative diffusion tracer V, with U being approximately lognormal:

$$P_{V|U}(v \mid u) \approx \mathrm{e}^{-(\ln v - m(u))^2/(2d(u))} \big/ (v\sqrt{2\pi d(u)}) \tag{11.5}$$

in the range $u^2 \ll v \ll 1$ corresponding to (11.2). Here, $m(u)$ and $d(u)$ are the mean and variance of the approximating conditional Gaussian probability distribution of $\ln V$ for a given $U = u > 0$. Self-similarity considerations combined with an associative consistency argument [16, section 3] applied to (11.4) suggest that

$$m(u) = m_1 \ln u, \qquad d(u) = -d_1 \ln u, \tag{11.6}$$

where m_1 and d_1 are positive parameters. The lognormal PDF describes the one-point distribution of a geometric Brownian motion (GBM)

$$\mathcal{V}(u) = \exp\Big(m_1 \ln u + \sqrt{d_1}\, \mathfrak{W}(-\ln u)\Big) \tag{11.7}$$

considered for $0 < u \leqslant 1$, where $\mathfrak{W}$ is a one-dimensional standard Wiener process and $-\ln u$ plays the role of fictitious time. Since $m_1 > 0$, the GBM $\mathcal{V}$ converges to zero with probability one as $u \to 0+$, thus reproducing the property that the diffusion tracer vanishes at the interface. Moreover, $\mathcal{V}$ multiplicatively responds to the rescaling of u in the sense that $\mathcal{V}(u_1)/\mathcal{V}(u_2)$ has the same lognormal distribution as $\mathcal{V}(u_1/u_2)$ for any $0 < u_1 \leqslant u_2 \leqslant 1$. The sole dependence of the distribution on the ratio u_1/u_2 holds in a more general model where m and d in (11.6) contain additive constants m_0 and d_0 that correspond to multiplying the subsidiary GBM $\mathcal{V}$ in (11.7)

by an independent lognormal random variable $\mathcal{V}_0$ whose logarithm has mean m_0 and variance d_0. We set the parameters m_0 and d_0 to zero since they can be "absorbed" by appropriately rescaling the arguments u and v of the lognormal PDF in (11.5), and the operation does not affect the exponent of the power law for P_V obtained below. Now, the conditional moments of V, suggested by (11.5) and (11.6), are

$$\langle V^\lambda \mid U = u \rangle \approx \mathrm{e}^{\lambda m(u) + \lambda^2 d(u)/2} = u^{m_1 \lambda - d_1 \lambda^2/2}. \tag{11.8}$$

In order for the right-hand side of (11.8) to be compatible with the inequality $V \geqslant U^2$ whereby $\langle V^\lambda \mid U = u \rangle \geqslant u^{2\lambda}$ for any $\lambda > 0$ and $u < 1$, the constant m_1 must satisfy

$$m_1 \leqslant 2. \tag{11.9}$$

Furthermore, by the physical meaning of U and V and from the hitting time interpretation of the diffusion tracer, the right-hand side of (11.8) must be nondecreasing in u for $\lambda = 1$, which implies

$$m_1 \geqslant d_1/2. \tag{11.10}$$

Finally, the lognormal approximation in (11.5) and (11.6) can be legitimate only if it ascribes negligible probability to the set $(0, u^2) \cup (1, +\infty)$ of prohibited values of V given $U = u$. This is equivalent to $\min(2 - m_1, m_1)\sqrt{|\ln u|/d_1} \gg 1$ and implies that the inequality on m_1 in (11.9) must be strict:

$$m_1 < 2. \tag{11.11}$$

Considering the case where the interface fractality dominates over the network fractality in the sense of (10.12), so that $P_U(u) \approx b u^{-a}$ in conformance with (10.10), where a is the interface excess dimension and b is given by (6.8), substitution of (11.5) and (11.6) into (10.4) gives

$$P_V(v) \approx \frac{b}{v} \int_0^{\sqrt{v}} u^{-a} \, (2\pi d_1 |\ln u|)^{-1/2} \, \mathrm{e}^{(\ln v - m_1 \ln u)^2/(2 d_1 \ln u)} \mathrm{d}u. \tag{11.12}$$

From the asymptotic analysis of the right-hand side of (11.12) in Appendix G, the PDF P_V essentially follows a power law

$$P_V(v) \propto v^{-\delta} \tag{11.13}$$

for $v \ll 1$, whose exponent is explicitly calculated therein in terms of b and the parameters m_1 and d_1 of the lognormal cascade hypothesis; see (G.7). The connection between the parameters m_1, d_1, and a to complement (11.10) and (11.11) is not straightforward and requires additional investigation.

12. Power law for diffusion tracer. We will now assemble the results of sections 9–11 to obtain the asymptotic behavior of the diffusion tracer PDF P_Z. Under the network distance-diffusion scaling hypothesis of (9.8), the intrinsic PDF of Z_* in (10.5) reads

$$P_{Z_*}(z_*) = \frac{1}{2}\sqrt{D/z_*} \int_{1/3}^{+\infty} P_Q(q) P_L(\sqrt{D z_*/q}) q^{-1/2} \mathrm{d}q, \tag{12.1}$$

where P_L is the intrinsic PDF of L defined by (9.3). Interpreting the power law of (10.8) as the intermediate asymptotic behavior of P_L with network fractality parameter α, (12.1) yields

$$P_{Z_*}(z_*) \sim \frac{(1-\alpha)}{2}(\sqrt{D}/L_{\text{out}})^{1-\alpha} z_*^{-(1+\alpha)/2} \int_{1/3}^{Dz_*/L_{\text{in}}^2} P_Q(q) q^{(\alpha-1)/2} \mathrm{d}q$$

$$\sim \frac{(1-\alpha)}{2}(\sqrt{D}/L_{\text{out}})^{1-\alpha} \left\langle Q(x)^{(\alpha-1)/2} \;\middle|\; x \in \Phi \right\rangle z_*^{-(1+\alpha)/2} \propto z_*^{-(1+\alpha)/2}, \tag{12.2}$$

provided that an overwhelming portion of the interval $[0, \sqrt{3Dz_*}]$ in (10.5) is in the monofractality range described by (5.1). Therefore, the power law of (12.2) should also be understood as an intermediate asymptotic behavior of $P_{Z_*}(z_*)$ in the range $L_{\text{in}}^2/D \ll z_* \ll L_{\text{out}}^2/D$. The same exponent, $-(1+\alpha)/2$, is predicted by the spherical pore approximation from (10.6). Now, combining the power law for P_{Z_*} in (12.2) with the power law for P_V in (11.13) which was obtained under the isolation of relative scales and lognormal cascade hypotheses, the diffusion tracer PDF P_Z in (10.3) follows the power law with the dominating exponent

$$P_Z(z) \propto z^{-c}, \qquad c := \max(\delta,\, (1+\alpha)/2). \tag{12.3}$$

As a corollary, consider the asymptotic behavior of the conditional Favre average $\overline{N}$ associated with (4.4). Recall that for incompressible fluids and D_0 constant, the conditional dissipation rate reduces to

$$\overline{N} := D_0 \left\langle |\nabla Z(x)|^2 \;\middle|\; Z(x) = z \right\rangle \tag{12.4}$$

and is related to the diffusion tracer PDF by the ODE

$$\partial_z(\overline{N} P_Z) = -W_0 P_Z \tag{12.5}$$

in the case where the fluid phase does not penetrate the solid matrix and the underlying random fields are all steady-state and spatially homogeneous; cf. [17, eq. (20), p. 2110] and (4.3) and (4.8) of the present work. Direct integration of (12.5) gives

$$\overline{N}(z) = (\text{const} - W_0 F_Z(z))/P_Z(z), \tag{12.6}$$

where $F_Z(z) := \mathsf{P}(0 < Z(x) < z)/\varphi = \int_0^z P_Z(u)\mathrm{d}u$ is the intrinsic cumulative distribution function of the diffusion tracer, and const is a positive constant. As the power law of (12.3) suggests, the ratio F_Z/P_Z in (12.6) is asymptotically linear in z with the coefficient completely determined by the exponent c,

$$\overline{N}(z) \approx \text{const} \times z^c - W_0 z/(1-c). \tag{12.7}$$

Here, const is another positive constant which governs the interplay between the fractional power, z^c, and linear, z, terms which balance each other at the point where the right-hand side of (12.7) achieves maximum. In addition to their significance for conditionally averaged transport equations of section 4, (12.3) and (12.7) can also be utilized for estimating the area $A(z)$ of the z-isosurface of Z per unit volume of the fluid phase. Indeed, it is computed as $A(z) = P_Z(z)\langle |\nabla Z| \mid Z = z\rangle$, and, by combining the Cauchy–Schwarz inequality [29] with (12.4), affords an upper bound $A \leqslant P_Z\sqrt{\overline{N}/D_0}$.

13. Conclusion. We have considered several aspects of the conditional averaging methods, which can be used for modeling of transport in two-component porous media with volume reactions in the fluid phase and surface reactions at the fluid/solid interface. Such methods follow the conditional moment closure (CMC) paradigm and employ the diffusion tracer as a reference scalar field to make the conditional averages sensitive to the proximity of a point in the fluid phase to the solid matrix near which the diffusion transport dominates over convection. The role of surface reactions and the near-interface region is especially important in porous media with well-developed fractal properties where both the interface and pores themselves manifest self-similarity in a wide range of spatial scales which amount to a significant portion of the fluid phase volume.

We have revised the conditionally averaged reactive transport equations of the PCMC approach, the adaptation of the CMC methodology to porous media, and established an ensemble version of the spatial averaging theorem using interface and inflow operators which facilitate the theoretical treatment of reactive flows across random surfaces. The ensemble averaging, together with related homogeneity and ergodicity issues, has been discussed in comparison with the conventional volume averaging. The near-interface behavior of the coefficients of the PCMC model is investigated for interfaces possessing fractal properties.

Since the conditionally averaged reactive transport equations are governed essentially by the PDF of the diffusion tracer, we have undertaken a systematic study of its behavior. The first hitting time stochastic representation of the diffusion tracer as a temporal measure of proximity to the solid matrix in terms of the three-dimensional Wiener process has been considered. Employing martingale and PDE techniques, we have established integral equations and a related Neumann series linking the diffusion tracer with the shortest distance to the solid matrix and obtained distance-diffusion inequalities. Higher moments of the first hitting time, forming a recurrence sequence initialized by the diffusion tracer, have also been considered.

We have qualitatively discussed fractality in porous media and utilized the contact dimension as a variant of the Minkowski–Bouligand fractal dimension to quantify the fractal properties of the fluid/solid interface in terms of the distance tracer, while fractality of pores themselves has been described using the network fractality parameter.

To investigate the interplay between the interface and network scenarios of fractality and their influence on the behavior of the diffusion tracer PDF, we have introduced the partition of the fluid phase into basins of attraction to local maxima of the diffusion tracer along the associated gradient flow. The maximum localization principle, closely related to the maximum principle for harmonic functions, has also been established. We have used the size of the resulting fragments of the fluid phase to rescale the diffusion and distance tracers so as to "decouple" the relative proximity to the interface from the pore largeness.

Due to the inherent complexity of the problem, our analysis has combined rigorous results with additional hypotheses which should be considered as heuristics for further development. We have conjectured the network distance-diffusion scaling and isolation of relative scales, with the latter hypothesis stochastically decoupling the effects of interface and network scenarios, and directly verified the hypotheses for spherical pores. The lognormal distribution of the relative diffusion tracer conditioned on the relative distance tracer, analogous to the lognormal energy cascade through eddies of different length scales in the statistical theory of turbulence, has also been conjectured.

Finally, as a main result of the present study, we have deduced a power law for the PDF of the diffusion tracer and calculated its exponent from the combined contribution of the interface and network scenarios of fractality, and we have outlined its implications for other characteristics relevant to conditionally averaged transport equations, particularly the conditional dissipation rate.

Appendix A. Ensemble averaging and ergodicity. The ensemble averages are, in general, not amenable to direct measurement. They can expose themselves (and be estimated) only through physically observable *spatial averages* over fragments of the porous medium—for example, *moving averages*. For a given nonnegative-valued *kernel function* K with bounded support, satisfying $\int_{\mathbb{R}^3} K(u)\mathrm{d}u = 1$, the K-weighted moving average of a function Y associated with the porous medium is defined by the convolution

$$\langle Y\rangle_K(x) := \int_{\mathbb{R}^3} K(x-u)Y(u)\mathrm{d}u. \tag{A.1}$$

If K is the appropriately normalized indicator of an averaging window centered at the origin, then the moving average $\langle\beta\rangle_K(x)$ of the fluid phase indicator in (3.1) is the volume fraction of the fluid phase within the window translated to x. The moving averages are *superficial averages* in that the integration in (A.1) involves not only the fluid phase, but also the solid matrix where those fields Y, which are defined only in the fluid phase, are padded with zero values. The latter convention is equivalent to defining $\langle Y\rangle_K$ for such fields as $\langle\beta Y\rangle_K$.

The random fields that occur in real-world systems are often only *locally* homogeneous in the sense that their ensemble characteristics are not strictly invariant under arbitrary translations of the space but are, nevertheless, almost constant on length scales bounded by a *homogeneity radius* L_h, which equals $+\infty$ in the case of ideal homogeneity. Another important index is the *correlation radius* L_c, which quantifies the characteristic length of decay in ensemble correlations, so that the values of the underlying random field at points, whose separation is $\gg L_\mathrm{c}$, are nearly independent in the sense of the ensemble probability measure.

Now, the extent to which the ensemble averages can be consistently estimated using the spatial averages, that is, the accuracy with which the latter can approximate the former, depends on the dimensionless quantity $L_\mathrm{h}/L_\mathrm{c}$. If this ratio is large, then it is possible to construct moving averages described by (A.1), with kernel functions K almost constant on length scales L_c and with support much smaller in linear size than L_h, which are good estimators for the local ensemble averages. For example, the moving average $\langle\beta\rangle_K$ of the fluid phase indicator with the kernel function $K := L^{-3}\mathcal{I}_Q$ associated with a cubic fragment Q of edge length L is a fairly accurate estimator of the local porosity of the medium in (3.2) if $L_\mathrm{c} \ll L \ll L_\mathrm{h}$. The ensemble root-mean-square value of its fluctuations behaves roughly as $(L_\mathrm{c}/L)^{3/2}$, which should be understood as an intermediate asymptotic.

In the case of ideal homogeneity, the convergence of the spatial averages to ensemble averages is known as *spatial ergodicity*, which, in the absence of detailed knowledge of the ensemble probability measure, can only be postulated. Thus, nonhomogeneous random fields may be treated as homogeneous ones over domains in the physical space whose size is well bounded by the homogeneity radius L_h, and the ergodicity may be considered to hold if it manifests itself well before the homogeneity breakdown.

Appendix B. Ensemble version of the spatial averaging theorem. Let Ξ be a linear operator which maps a scalar- or vector-valued random field ξ to a

deterministic function $\Xi(\xi)$ defined as the Radon–Nikodým derivative (density) of the countably additive measure

$$\left\langle \int_{A\cap\partial\Phi} \xi \mathrm{d}s \right\rangle = \int_A \Xi(\xi)\mathrm{d}x \tag{B.1}$$

on volume measurable sets $A \subset \mathbb{R}^3$, assuming that the measure is absolutely continuous. Here, ξ needs to be defined at least at the fluid/solid interface $\partial\Phi$. The surface integral on the left-hand side of (B.1) is taken over the fragment of the interface contained by A. The map Ξ will be referred to as the *interface operator*. For example, applied to the identically unit field, $\Xi(1)(x)$ is the average interface area per unit volume of the porous medium in the infinitesimal vicinity of a point x. Furthermore, $\Xi(f\xi) = f\Xi(\xi)$ for any *nonrandom* continuous scalar field f.

The ensemble version of the spatial averaging theorem [32, p. 10], which we establish below, is concerned with a random vector field G whose realizations are continuously differentiable on the fluid phase set Φ and continuous on the closure $[\Phi] := \Phi \cup \partial\Phi$. Note that the indicator function β in (3.1) and G are not required to be statistically independent and homogeneous. Assuming that f is an infinitely differentiable nonrandom scalar-valued test function with bounded support, and using integration by parts, commutativity of the ensemble averaging $\langle\cdot\rangle$ with spatial integration over a nonrandom set, and the divergence theorem, we have

$$\begin{aligned}
\int_{\mathbb{R}^3} f\mathrm{div}\langle\beta G\rangle \mathrm{d}x &= -\int_{\mathbb{R}^3} \langle\beta G\rangle\cdot\nabla f \mathrm{d}x = -\left\langle \int_{\mathbb{R}^3} \beta G\cdot\nabla f \mathrm{d}x\right\rangle = -\left\langle \int_\Phi G\cdot\nabla f \mathrm{d}x\right\rangle \\
&= \left\langle \int_\Phi f\mathrm{div}G\mathrm{d}x\right\rangle - \left\langle \int_\Phi \mathrm{div}(fG)\mathrm{d}x\right\rangle \\
&= \left\langle \int_{\mathbb{R}^3} f\beta\mathrm{div}G\mathrm{d}x\right\rangle + \left\langle \int_{\partial\Phi} fG\cdot\nu\mathrm{d}s\right\rangle \\
&= \int_{\mathbb{R}^3} f\langle\beta\mathrm{div}G\rangle\mathrm{d}x + \int_{\mathbb{R}^3} f\Xi(G\cdot\nu)\mathrm{d}x,
\end{aligned} \tag{B.2}$$

where ν is the unit normal at $\partial\Phi$ towards the fluid phase, and use is also made of the interface operator Ξ introduced by (B.1). Here, the function

$$\Upsilon(G) := \Xi(G\cdot\nu) \tag{B.3}$$

describes the local average inflow of the vector field G across the interface into the fluid phase per unit volume of the porous medium. By the validity of (B.2) for any test function f, with the *inflow operator* Υ defined by (B.3), the ensemble version of the spatial averaging theorem takes the form

$$\mathrm{div}\langle\beta G\rangle = \langle\beta\mathrm{div}G\rangle + \Upsilon(G).$$

Appendix C. Higher moments of first hitting time. The conditional PDF $q(t,x)$ of the first hitting time $\tau(x)$, defined by (7.1), for a given realization of the fluid phase set Φ, contains more information on the relative position of a point $x \in \Phi$ with respect to the solid matrix and the local structure of the interface $\partial\Phi$ than that provided by its first moment described by the diffusion tracer $Z(x) = \int_0^{+\infty} tq(t,x)\mathrm{d}t$ in (7.2). Consider the moment generating function given by the Laplace transform of the PDF:

$$M_\lambda(x) := \mathsf{E}\mathrm{e}^{-\lambda\tau(x)} = \int_0^{+\infty} \mathrm{e}^{-\lambda t} q(t,x)\mathrm{d}t, \tag{C.1}$$

where $\lambda \geqslant 0$. Since the probability of the random event $\{\tau(x) < \varepsilon\}$ is $o(\varepsilon)$ as $\varepsilon \to 0+$, the Markov property of the standard Wiener process $\mathcal{W}$ yields $M_\lambda(x) = \mathrm{e}^{-\lambda\varepsilon}\mathsf{E}M_\lambda(x+\sqrt{D}\mathcal{W}(\varepsilon))+o(\varepsilon)$. Hence, in view of the expansion $\mathsf{E}M_\lambda(x+\sqrt{D}\mathcal{W}(\varepsilon)) = M_\lambda(x) + \varepsilon D\Delta M_\lambda(x)/2 + o(\varepsilon)$, which can be obtained by averaging the quadratically truncated Taylor series for M_λ in the vicinity of x and is closely related to $\Delta/2$ being the infinitesimal generator [25, pp. 123–124] of $\mathcal{W}$, the function M_λ satisfies the screened Laplace equation

$$\Delta M_\lambda(x) = 2\lambda M_\lambda(x)/D, \qquad x \in \Phi, \tag{C.2}$$

with unit boundary condition $M_\lambda|_{\Phi^{\mathrm{C}}} = 1$; see [11] for more details. Using (C.1) and matching the appropriate terms of the Taylor series expansions for both parts of (C.2) for small λ shows that the kth moment $Z_k(x) := \mathsf{E}(\tau(x)^k) = (-1)^k\partial_\lambda^k M_\lambda(x)|_{\lambda=0}$ of the first hitting time (with $Z_0 \equiv 1$) satisfies the Poisson PDE with zero boundary condition:

$$\Delta Z_k(x) = -2kZ_{k-1}(x)/D, \quad x \in \Phi; \qquad Z_k|_{\Phi^{\mathrm{C}}} = 0.$$

The first of these recurrent equations (with $k = 1$) is (7.3) for the diffusion tracer $Z_1 \equiv Z$.

Appendix D. Second contact sphere. Since the right-hand side of (8.8) is quadratic in the distance tracer R, it provides a poor lower bound for the diffusion tracer Z near those points of the interface $\partial\Phi$ where $|\nabla Z| \neq 0$. In particular, the latter holds at any smoothness point of the interface. In order to improve the distance-diffusion inequality, denote by $R_*(x)$ the largest radius r of a sphere $\partial B(c, r)$ (with an arbitrary center c) which encloses the contact sphere $\Sigma(x)$, defined by (6.2), but, at the same time, is contained, along with the enclosed ball $B(c, r)$, by the closure $[\Phi]$ of the fluid phase set: $B(x, R(x)) \subset B(c, r) \subset \Phi$. Since $\Sigma(x)$ itself satisfies these two requirements, then $R_*(x) \geqslant R(x)$. The last inequality becomes an equality if, for example, the set of nearest points of the solid matrix, $\Theta(x) := \mathrm{Arg}\,\min_{y\in\Phi^{\mathrm{C}}}|x - y|$, consists of more than one element. Such points $x \in \Phi$ are, however, exceptional, usually constituting a negligible set of volume zero. Consider therefore the general situation where $\Theta(x)$ is a singleton. In this case, the above-mentioned sphere of radius $R_*(x)$ is tangent to the contact sphere $\Sigma(x)$ at the point $\Theta(x)$ and is described by

$$\Sigma_*(x) := \partial B\left(C(x), R_*(x)\right), \tag{D.1}$$

where the center

$$C(x) := \Theta(x) + R_*(x)(x - \Theta(x))/R(x) \tag{D.2}$$

belongs to the straight line passing through x and $\Theta(x)$; see Figure D.1. Both $\Sigma(x)$ and $\Sigma_*(x)$, with the latter referred to as the *second contact sphere*, are supported by the same tangent plane to $\partial\Phi$ at $\Theta(x)$. Since $\Sigma_*(x)$ encloses $\Sigma(x)$, then applying (8.2) and the hitting time argument of section 8 to $\Sigma_*(x)$ yields a stronger lower bound for the diffusion tracer,

$$\begin{aligned} Z(x) &= (2R_*(x) - R(x))R(x)\left(\frac{1}{3D} + \frac{1}{4\pi R_*(x)}\int_{\Sigma_*(x)}\frac{Z(s)}{|s-x|^3}\mathrm{d}s\right) \\ &\geqslant (2R_*(x) - R(x))R(x)/(3D) = \mathsf{E}\tau_*(x). \end{aligned} \tag{D.3}$$

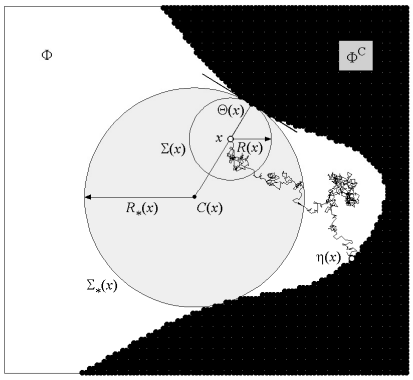

FIG. D.1. *A cross section of the contact spheres described by* (6.2) *and* (D.1) *for a point x in the fluid phase Φ. The second contact sphere $\Sigma_*(x)$ with radius $R_*(x)$ and center $C(x)$, given by* (D.2)*, is tangent to the first contact sphere $\Sigma(x)$ at the interface point $\Theta(x)$, nearest to x. Also shown is a sample path of the Brownian motion $x + \sqrt{D}\mathcal{W}$ stopped at the first hitting point $\eta(x)$.*

The right-hand side of this inequality is the expected value of the time $\tau_*(x) := \min\{t \geqslant 0 : x + \sqrt{D}\mathcal{W}(t) \in \Sigma_*(x)\}$ needed for the Brownian motion to reach $\Sigma_*(x)$ for a given realization of Φ. Equation (D.3) implies that the boundary value of $|\nabla Z|$ at a smoothness point y of the interface $\partial\Phi$ satisfies

$$|\nabla Z(y)| = \lim_{x \to y:\ x \in \Phi} (Z(x)/R(x)) \geqslant 2R_*(y)/(3D), \tag{D.4}$$

where $R_*(y)$ is the largest radius of a sphere passing through y and contained, along with the enclosed ball, by $[\Phi]$. Although the right-hand side of (D.4) is only a lower bound, it is qualitatively correct in predicting small values for $|\nabla Z|$ near the bottom of a deep cavity in the solid matrix—which is an efficient trap for the Brownian motion, thus shortening the hitting time—and large values for $|\nabla Z|$ near the tip of an outstanding ledge which is easily escapable, thereby delaying the collision with the solid matrix; see Figure D.2.

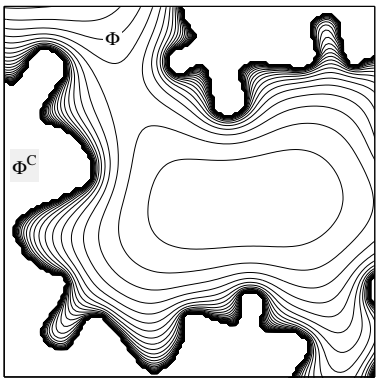

FIG. D.2. *A cross section of isosurfaces of the diffusion tracer Z on a logarithmic level scale. The isolines are well spaced and $|\nabla Z|$ is small near bottoms of deep cavities in the solid matrix which are reachable only from close vicinity. At the same time, $|\nabla Z|$ is large and the isolines of Z are dense near tips of outstanding ledges which are widely accessible to their surroundings.*

Appendix E. Maximum localization principle. The *maximum localization principle*, which we establish below, is closely related to the maximum principle for harmonic functions [31, section 24 in Chapter V]. Let an open ball $B(c,r)$ of positive radius r be contained by the fluid phase set Φ. If the oscillation of the diffusion tracer Z on the sphere $\partial B(c,r)$ is relatively small in the sense that

$$\zeta := \max_{y\in\partial B(c,r)} Z(y) - \min_{y\in\partial B(c,r)} Z(y) < r^2/(3D), \tag{E.1}$$

then the maximum of Z over the closure of the ball is achieved in a concentric ball of smaller radius $\sqrt{3D\zeta}$,

$$\max_{y\in[B(c,r)]} Z(y) = \max_{y\in[B(c,\sqrt{3D\zeta})]} Z(y). \tag{E.2}$$

Indeed, since the normalized surface integral on the right-hand side of (8.1) is not less than $\min_{y\in\partial B(c,r)} Z(y)$, then

$$Z(c) \geqslant r^2/(3D) + \min_{y\in\partial B(c,r)} Z(y). \tag{E.3}$$

On the other hand, (8.2) implies that

$$Z(x) \leqslant (r^2 - |x-c|^2)/(3D) + \max_{y\in\partial B(c,r)} Z(y) \tag{E.4}$$

for any $x \in B(c,r)$. Therefore, if $|x-c| > \sqrt{3D\zeta}$, then from (E.1), (E.3), and (E.4),

$$Z(x) < r^2/(3D) - \zeta + \max_{y\in\partial B(c,r)} Z(y) \leqslant Z(c). \tag{E.5}$$

Since $\max_{y\in[B(c,\sqrt{3D\zeta})]} Z(y) \geqslant Z(c)$, then this maximum exceeds the values of Z in the spherical layer $[B(c,r)] \setminus [B(c,\sqrt{3D\zeta})]$ which, by (E.5), are all less than $Z(c)$. Hence, (E.2) follows.

Appendix F. Toy example: Spherical pores. We will directly verify the network distance-diffusion scaling and isolation of relative scales hypotheses of sections 9 and 10 for an illustrative example below where the fluid phase set Φ consists of nonoverlapping spherical pores; see Figure F.1. The boundary of the pore containing a given point $x \in \Phi$ coincides with the second contact sphere $\Sigma_*(x)$ defined in Appendix D, and hence the radius of the pore is $R_*(x)$, which, in turn, coincides with $L(x)$ from (9.3) in the case of spherical pores considered. Since the integral in (D.3) vanishes here, the diffusion tracer affords the explicit representation

$$Z(x) = (2L(x) - R(x))R(x)/(3D), \tag{F.1}$$

whence the allied function Z_* defined by (9.2) reads

$$Z_*(x) = L(x)^2/(3D), \tag{F.2}$$

thereby making the ratio Q from (9.7) identically equal to $1/3$ and trivially independent of L. The latter justifies the network distance-diffusion scaling hypothesis in this case. Furthermore, assuming the random fields homogeneous for simplicity and combining geometric probability considerations with an ergodicity argument, the joint PDF of the random variables $R(x)$ and $L(x)$ is

$$P_{R,L}(r,\ell) = 3(\ell - r)^2\ell^{-3}P_L(\ell), \qquad 0 < r < \ell, \tag{F.3}$$

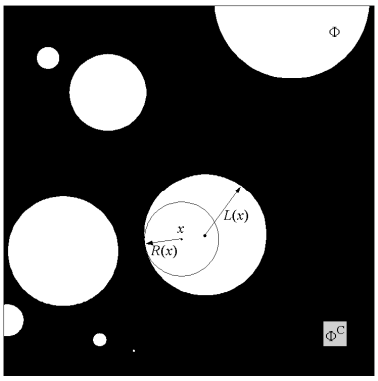

FIG. F.1. *An illustrative example of a porous medium with nonoverlapping spherical pores. The radius $L(x)$ of the pore that contains a point x of the fluid phase Φ is the radius $R_*(x)$ of the second contact sphere $\Sigma_*(x)$ which coincides with the boundary of the pore.*

where P_L is the intrinsic PDF of $L(x)$. Indeed, consider a large fragment of the model porous medium where the fluid phase occupies volume Ω. The total volume of those pores, whose radius belongs to an infinitesimal interval $[\ell, \ell + \mathrm{d}\ell]$, is $\Omega P_L(\ell)\mathrm{d}\ell$, and hence the number of them is $\Omega P_L(\ell)\mathrm{d}\ell/(4\pi\ell^3/3)$. In each of these pores, those points x, whose distance $R(x)$ to the solid matrix is in another infinitesimal interval $[r, r + \mathrm{d}r]$, form a spherical layer of volume $4\pi(\ell - r)^2\mathrm{d}r$. Therefore, multiplying the latter volume by the number of the selected pores gives the volume of those points x of the confined fluid phase where the pair $(R(x), L(x))$ belongs to the Cartesian product of the above intervals $[r, r + \mathrm{d}r] \times [\ell, \ell + \mathrm{d}\ell]$. On the other hand, the resulting volume is $4\pi(\ell - r)^2\mathrm{d}r\,\Omega P_L(\ell)\mathrm{d}\ell\big/(4\pi\ell^3/3) = \Omega P_{R,L}(r, \ell)\mathrm{d}r\mathrm{d}\ell$, which yields (F.3). Now, the latter implies that the ratio U from (10.1) is independent of L and has PDF $3(1-u)^2$ on the unit interval $0 < u < 1$. Hence, the second ratio V from (10.1), which, in view of (F.1) and (F.2), takes the form $V(x) = U(x)(2 - U(x))$, is also independent of $L(x)$, thereby establishing the isolation of relative scales hypothesis in the example considered. This derivation shows that the sphericity of pores is not crucial but merely simplifies calculation, while their disjointness is indeed important. It seems, however, reasonable to expect that if the pores are connected by relatively small channels, then the network distance-diffusion scaling and isolation of relative scales are only slightly distorted.

Appendix G. Asymptotic behavior of the relative diffusion tracer PDF. To investigate the approximation of the PDF P_V of the relative diffusion tracer provided by (11.12) under the lognormal cascade hypothesis of section 11, we introduce a new integration variable $w \geqslant 1/2$ via the substitution $u := v^w$ which gives

$$P_V(v) \approx \frac{b}{v}\int_0^{\sqrt{v}} u^{-a}\,(2\pi d_1|\ln u|)^{-1/2}\,\mathrm{e}^{(\ln v - m_1 \ln u)^2/(2d_1 \ln u)}\mathrm{d}u$$

$$= b\sqrt{|\ln v|/(2\pi d_1)}\,v^{-(\frac{m_1}{d_1}+1)}\int_{1/2}^{+\infty} v^{f(w)}w^{-1/2}\mathrm{d}w, \tag{G.1}$$

with

$$f(w) := \big(b + m_1^2/(2d_1)\big)\,w + 1/(2d_1 w). \tag{G.2}$$

The rightmost integral in (G.1) is amenable to asymptotic analysis for $v \ll 1$ using Laplace's method [9]. The minimum

$$\widehat{f} := \min_{w \geqslant 1/2} f(w) = f(\widehat{w}) = \frac{1}{d_1} \times \begin{cases} \sqrt{m_1^2 + 2bd_1} & \text{if } m_1^2 + 2bd_1 < 4, \\ 1 + (m_1^2 + 2bd_1)/4 & \text{otherwise} \end{cases} \tag{G.3}$$

is achieved at the unique point

$$\widehat{w} := 1/\min\left(2, \sqrt{m_1^2 + 2bd_1}\right). \tag{G.4}$$

If $m_1^2 + 2bd_1 < 4$, which is a stronger condition than (11.11), then $\widehat{w}$ is a critical point of f in (G.2), in the vicinity of which the quadratic approximation $f \approx \widehat{f} + (w-\widehat{w})^2/(2d_1\widehat{w}^3)$ ensures that $v^{f(w)} = \exp(-|\ln v| f(w))$ in (G.1) is proportional, with good accuracy, to the Gaussian PDF with mean $\widehat{w}$ and small variance $d_1\widehat{w}^3/|\ln v|$. Hence, Laplace's method yields

$$\int_{1/2}^{+\infty} v^{f(w)} w^{-1/2} \mathrm{d}w \sim \widehat{w}\, \sqrt{2\pi d_1/|\ln v|}\, v^{\widehat{f}}, \qquad v \to 0+. \tag{G.5}$$

Alternatively, if $m_1^2 + 2bd_1 > 4$, then (G.4) gives $\widehat{w} = 1/2$ and the minimum is achieved at the left endpoint of the integration interval in the unilateral vicinity of which f is well approximated by the linear function $\widehat{f} + f'(1/2)(w - 1/2)$ with positive slope $f'(1/2) = b + (m_1^2 - 4)/(2d_1)$, so that $v^{f(w)}$ is proportional to an exponential PDF, again with a small variance, resulting in

$$\int_{1/2}^{+\infty} v^{f(w)} w^{-1/2} \mathrm{d}w \sim \sqrt{2}\, v^{\widehat{f}} / (f'(1/2)|\ln v|), \qquad v \to 0+. \tag{G.6}$$

Excluding the special situation $m_1^2 + 2bd_1 = 4$ from analysis and combining (G.5) and (G.6) with (G.1) shows that in both cases the PDF P_V asymptotically follows the power law

$$P_V(v) \approx b v^{-\delta} \times \begin{cases} \widehat{w} & \text{if } m_1^2 + 2bd_1 < 4, \\ \left(f'(1/2)\sqrt{\pi d_1 |\ln v|}\right)^{-1} & \text{if } m_1^2 + 2bd_1 > 4, \end{cases} \qquad v \ll 1,$$

which, in the second case, is slightly tempered by a logarithmically small factor $\propto |\ln v|^{-1/2}$. The exponent of this power law is expressed in terms of the minimum value $\widehat{f}$ from (G.3) as

$$\delta := 1 + m_1/d_1 - \widehat{f}. \tag{G.7}$$

Acknowledgment. The authors are grateful to the anonymous reviewers for useful comments.

REFERENCES

[1] P. Adler, *Flow in porous media*, in Fractal Approach to Heterogeneous Chemistry, D. Avnir, ed., Wiley, Chichester, UK, 1989, pp. 341–359.

[2] G. I. Barenblatt, *Scaling, Self-Similarity, and Intermediate Asymptotics*, Cambridge University Press, New York, 1996.

[3] C. Barton and P. L. Pointe, eds., *Fractals in Petroleum Geology and Earth Processes*, Plenum Press, New York, 1995.
[4] A. Bejan, *Convection Heat Transfer*, 3rd ed., Wiley, Hoboken, NJ, 2004.
[5] J. L. P. Bernal and M. A. B. Lopez, *The fractal dimension of stone pore surface as weathering descriptor*, Appl. Surface Sci., 161 (2000), pp. 47–53.
[6] R. W. Bilger, *Marker fields for turbulent premixed combustion*, Combust. Flame, 138 (2004), pp. 188–194.
[7] B. Dubuc, J. F. Quiniou, C. Roques-Carmes, C. Tricot, and S. W. Zucker, *Evaluating the fractal dimension of profiles*, Phys. Rev. A, 39 (1989), pp. 1500–1512.
[8] K. J. Falconer, *The Geometry of Fractal Sets*, Cambridge University Press, Cambridge, UK, 1985.
[9] M. V. Fedoryuk, *Asymptotic Analysis*, Springer, Berlin, 1992.
[10] J. F. Fleron, *Gabriel's wedding cake*, College Math. J., 30 (1999), pp. 35–38.
[11] I. I. Gikhman and A. V. Skorokhod, *The Theory of Stochastic Processes*, Springer, Berlin, 1974.
[12] W. G. Gray and S. M. Hassanizadeh, *Averaging theorems and averaged equations for transport of interface properties in multiphase systems*, Int. J. Multiphase Flow, 15 (1989), pp. 81–95.
[13] R. Hilfer, *Transport and relaxation phenomena in porous media*, in Advances in Chemical Physics, I. Prigogine and S. A. Rice, eds., Wiley, New York, 1996, pp. 299–423.
[14] I. Karatzas and S. E. Shreve, *Brownian Motion and Stochastic Calculus*, Springer, New York, 1988.
[15] D. G. Kendall, *Foundations of a theory of random sets*, in Stochastic Geometry, E. F. Harding and D. G. Kendall, eds., Wiley, New York, 1974, pp. 322–376.
[16] A. Y. Klimenko, *Examining the cascade hypothesis for turbulent premixed combustion*, Combust. Sci. Tech., 139 (1998), pp. 15–40.
[17] A. Y. Klimenko and M. M. Abdel-Jawad, *Conditional methods for continuum reacting flows in porous media*, Proc. Combustion Institute, 31 (2007), pp. 2107–2115.
[18] A. Y. Klimenko and R. W. Bilger, *Conditional moment closure for turbulent combustion*, Progr. Energy Combust. Sci., 25 (1999), pp. 595–687.
[19] A. N. Kolmogorov, *A refinement of previous hypotheses concerning the local structure of turbulence in a viscous incompressible fluid at high Reynolds number*, J. Fluid Mech., 13 (1962), pp. 82–85.
[20] R. Lenormand, *Applications of fractal concepts in petroleum engineering*, Phys. D, 38 (1989), pp. 230–234.
[21] B. Mandelbrot, *The Fractal Geometry of Nature*, W. H. Freeman, San Francisco, 1982.
[22] K. Z. Markov, *On the correlation functions of two-phase random media and related problems*, R. Soc. Lond. Proc. Ser. A Math. Phys. Eng. Sci., 455 (1999), pp. 1049–1066.
[23] G. de Marsily, *Quantitative Hydrogeology*, Academic Press, New York, 1986.
[24] G. Matheron, *Random Sets and Integral Geometry*, Wiley, New York, 1975.
[25] B. Øksendal, *Stochastic Differential Equations: An Introduction with Applications*, 6th ed., Springer, Berlin, 2005.
[26] B. Øksendal and D. W. Stroock, *A characterization of harmonic measure and Markov processes whose hitting distributions are preserved by rotations, translations and dilatations*, Ann. Inst. Fourier (Grenoble), 32 (1982), pp. 221–232.
[27] K. Oleschko, J.-F. Parrot, G. Ronquillo, S. Shoba, G. Stoops, and V. Marcelino, *Weathering: Toward a fractal quantifying*, Math. Geol., 36 (2004), pp. 607–627.
[28] L. C. G. Rogers and D. Williams, *Diffusions, Markov Processes and Martingales*, Cambridge University Press, Cambridge, UK, 2000.
[29] A. N. Shiryaev, *Probability*, 2nd ed., Springer, New York, 1996.
[30] H. E. Stanley and P. Meakin, *Multifractal phenomena in physics and chemistry*, Nature, 335 (1988), pp. 405–409.
[31] V. S. Vladimirov, *Equations of Mathematical Physics*, Mir, Moscow, 1984.
[32] S. Whitaker, *The Method of Volume Averaging*, Kluwer Academic Publishers, Dordrecht, The Netherlands, 1999.